Journal of Hydrology: Regional Studies 63 (2026) 103063

Contents lists available at ScienceDirect

Journal of Hydrology: Regional Studies

journal homepage: www.elsevier.com/locate/ejrh

How earthquakes reshape carbonate aquifers: Modelling groundwater redistribution in Central Italy after the October 2016, M_w 6.5 Norcia earthquake

Enrica Zullo [a,b], Matteo Albano [c,*], Michele Saroli [a,b,c], Marco Moro [c], Gabriel Testa [a,b], Marco Petitta [d], Nicola Bonora [a,b], Thomas Reimann [e], Carlo Doglioni [d]

[a] Dipartimento di Ingegneria Civile e Meccanica, Università degli Studi di Cassino e del Lazio meridionale, via G. di Biasio 43, 03043 Cassino, Italy
[b] European University of Technology EUt+, European Union, Italy
[c] Istituto Nazionale di Geofisica e Vulcanologia, via di Vigna Murata 605, 00143 Roma, Italy
[d] Dipartimento di Scienze della Terra, "Sapienza" Università di Roma, p.le Aldo Moro 5, 00185 Roma, Italy
[e] Institut für Grundwasserwirtschaft, Technische Universität Dresden, Bergstraße 66, 01062 Dresden, Germany

ARTICLE INFO

Keywords:
Groundwater flow numerical modelling
Carbonate hydrostructure
Earthquake
Active faults

ABSTRACT

Study region: The carbonate hydrostructures of the Italian Apennines host major aquifers that serve as a critical groundwater resource. In tectonically active settings, such as the *Sibillini* Mountains, structural discontinuities and deformation features exert a dominant control on the hydraulic conductivity and storage properties of aquifers, thereby modulating groundwater flow regimes.
Study focus: The M_w 6.5 Norcia earthquake of October 30th 2016, part of the 2016 Central Italy seismic sequence, caused extensive ground deformation and surface faulting, triggering significant and long-lasting hydrogeological changes across the *Sibillini* Mountains carbonate aquifer. In this study, we develop a regional-scale conceptual hydrogeological model and implement it in steady-state numerical simulations. Our modelling reproduces pre- and post-seismic groundwater flow conditions and highlights the role of major active faults in governing aquifer hydrodynamics.
New hydrological insights for the region: Simulations demonstrate that the earthquake-induced fault rupture, modelled as a binary (on-off) feature, facilitated cross-fault groundwater transfer, leading to a persistent depletion of the eastern aquifer sector and enhanced discharge in the central and western sectors. These findings provide evidence of how seismic events can reconfigure groundwater flow patterns in fractured carbonate systems, highlighting the critical role of tectonic structures in controlling their hydrodynamic balance.

1. Introduction

Over the last century, recurring changes in hydrogeological regimes induced by strong earthquakes have increasingly captured the interest of scientists, fascinated by the complex nature of the processes that govern aquifer responses and their evolution over time

* Corresponding author.
E-mail address: matteo.albano@ingv.it (M. Albano).

https://doi.org/10.1016/j.ejrh.2025.103063
Received 12 June 2025; Received in revised form 5 November 2025; Accepted 16 December 2025
Available online 19 December 2025

(Manga et al., 2012). These changes include water level fluctuations in wells (Ingebritsen and Manga, 2019; Wakita, 1975), changes in stream discharge, the appearance and disappearance of springs (Manga and Wang, 2015; Montgomery and Manga, 2003; Muir-Wood and King, 1993), and changes in groundwater properties such as colour, temperature and chemical composition (Li et al., 2019).

Such phenomena were observed following several earthquakes worldwide. The M_w 9.2 Great Alaska Earthquake in 1964 (Hansen et al., 1966) caused groundwater level fluctuations recorded even hundreds of kilometres from the epicentre, while in the near field, wells exhibited turbidity spikes associated with these oscillations (Vorhis et al. 1967 and references therein). The 1995 Kobe earthquake (Japan) produced a rapid and sustained increase in discharge at springs along the active fault system, accompanied by a drop in water levels at high-altitude wells (Sato et al., 2000). Similar manifestations were observed in the epicentral area of the 2014 M_w 6.0 Napa and the 2007 M_w 5.5 Alum Rock earthquake (California (Manga and Rowland, 2009; Manga and Wang, 2015)), and during the 2016 seismic sequence in Central Italy (Mastrorillo et al., 2020; Petitta et al., 2018; Valigi et al., 2019), where rapid variations in the discharge rate at springs occurred. Many previously dry streams and springs began to flow again, while some springs showed permanent changes in discharge rate.

In 2023, two significant earthquakes (M_w 7.7 and 7.6) in Turkey caused a 430 km surface rupture, disrupting groundwater systems and compromising potable water quality. The increase in groundwater discharge at karst springs was linked to elevated turbidity, suggesting the presence of microbial pathogens (ŞiMşek et al., 2024).

Additional manifestations related to groundwater include soil liquefaction and the formation of mud volcanoes and geysers (Manga et al., 2012). An example of these phenomena has been observed during the 2012 seismic sequence that occurred in the alluvial valley of the Po Plain in Northern Italy. Although the two M_w 6.0 and 5.8 reverse fault events did not produce coseismic surface faulting, they caused strong seismic motion that triggered significant liquefaction, resulting in the ejection of sand from ground cracks and water wells, as well as local differential subsidence (Albano et al., 2024; Emergeo Working Group, 2013; Papathanassiou et al., 2015).

These hydrologic responses occur over a wide range of timescales, from as short as the duration of shaking to permanent changes, and over a wide range of length scales, from within the fault zone to more than 10.000 km away (Albano et al., 2024; Brodsky et al., 2003; De Luca et al., 2018; Isaya et al., 2025; Manga, 2001; Muir-Wood and King, 1993; Rojstaczer et al., 1995; Shi et al., 2019; Wakita, 1975; Wang et al., 2003).

Hydrological effects arise from the properties of the Earth's crust, which acts as a poroelastic medium (Wang, 2000). This medium consists of a solid framework and voids occupied by fluids (Albano et al., 2019; Fyfe, 1978). In shallower, compartmentalised hydrogeological systems, seismogenic faults often serve as relative hydraulic barriers (Bense et al., 2013), obstructing fault-orthogonal groundwater flow and hydraulically isolating the system's compartments. During earthquakes, fault slip could disrupt this barrier effect, enabling groundwater to flow through the fault (Manga et al., 2012; Manga and Wang, 2015; Mastrorillo et al., 2020). Moreover, coseismic static stress changes and dynamic stresses caused by seismic waves create static and dynamic volumetric strains at the surface and within seismogenic depths. Consequently, this leads to alterations in hydraulic gradients, shifts in groundwater divides, and changes in permeability and storage characteristics of underground structures, resulting in water-level fluctuations in wells and changes in spring and streamflow discharge rates.

These phenomena have scientific significance because they demonstrate the dual interaction between earthquakes and fluids, thereby facilitating the development of theoretical formulations that, in principle, should also describe the more subtle manifestations occurring before earthquakes (Albano et al., 2021b, 2021a; Moro et al., 2017). Furthermore, in an age when climate change undermines both the quantity and quality of available water resources, tectonic activity poses a considerable risk, not only due to the direct damage to human lives and infrastructure but also concerning the availability and sustainable management of drinking water.

Despite extensive research and the development of integrated, widely accepted hypotheses explaining seismic-related hydrogeological changes, key uncertainties remain. Fundamental questions persist: when will hydrodynamic equilibrium be restored? Will the system return to pre-seismic conditions, and if not, why? What future changes may follow another earthquake?

In recent years, numerical modelling of groundwater flow has become increasingly important not only for understanding and predicting the recharge-discharge processes of diffuse-flow karst systems and managing groundwater resources (Leone et al., 2025) but also for understanding and anticipating critical scenarios, including those triggered by seismic events (Lancia et al., 2020; Parsasadr et al., 2024; Scharling et al., 2009). Hydrogeological models, particularly those incorporating fault systems, offer valuable insights into groundwater behaviour under stress. However, simulating fault-related flow remains complex due to geological heterogeneity and transient seismic effects.

To date, no regional-scale models have been developed to simulate earthquake-induced changes in groundwater flow. This gap stems from the complex, poorly constrained nature of earthquake-groundwater interactions.

Numerical models fundamentally rely on conceptual models. A conceptual hydrogeological model is a simplified yet scientifically sound representation of the key geological and hydrological processes controlling groundwater flow (Anderson et al., 2015; Enemark, 2020; Kresic and Mikszewski, 2012). Its development depends on the study's purpose (Reilly and Harbaugh, 2004), such as examining existing conditions or forecasting future ones, and integrates geological, hydrogeological, and geochemical data to describe subsurface structures, hydraulic properties, recharge and discharge mechanisms, and interactions with surface water. It outlines hydrostratigraphic units and flow types, providing the basis for numerical modelling and predictive analysis.

This research aims to clarify the influence of fault rupture on groundwater dynamics by reconstructing pre- and post-seismic groundwater flow conditions through an integrated conceptual and numerical modelling approach. Specifically, we examine the impact of the M_w 6.5 earthquake in Central Italy on October 30th, 2016, which significantly affected the groundwater flow directions and discharge rates of the *Sibillini* Mts hydrogeological system (Fig. 1). We first analysed persistent groundwater changes that modified the regional aquifer by collecting and analysing all available literature data. Then, we developed a sound hydrogeological conceptual model, which enabled us to provide a qualitative description of the hydrogeological system's behaviour before and after the

earthquake sequence. We applied this conceptual model to perform a numerical analysis of the groundwater system. The proposed approach and methods allowed us to simulate groundwater flow at varying levels of complexity before and after the earthquake. This approach allowed us to explore the system's behaviour and verify the hypotheses about the mechanisms controlling the observed changes in groundwater flow.

2. The study area

2.1. Tectonic and hydrogeological setting

The *Sibillini* Mountains (Fig. 1a) form part of the east-verging fold-and-thrust belt of the Central Apennines, developed during the late Miocene to early Pliocene compressional phase (Lavecchia et al., 1988). This morpho-structural framework results from the deformation of a 2-km-thick Meso-Cenozoic sedimentary succession, deposited in a passive-margin setting associated with the southern Tethys Ocean. The stratigraphy mainly comprises carbonate lithologies, reflecting a transition from platform to basin environments. The frontal structure of the *Sibillini* ridge is the asymmetric, east-verging anticline of *Vettore* Mt, whose eastern limb is dissected by the *Sibillini* Mountains thrust system (SMt), the main regional contractional structure separating the carbonate platform

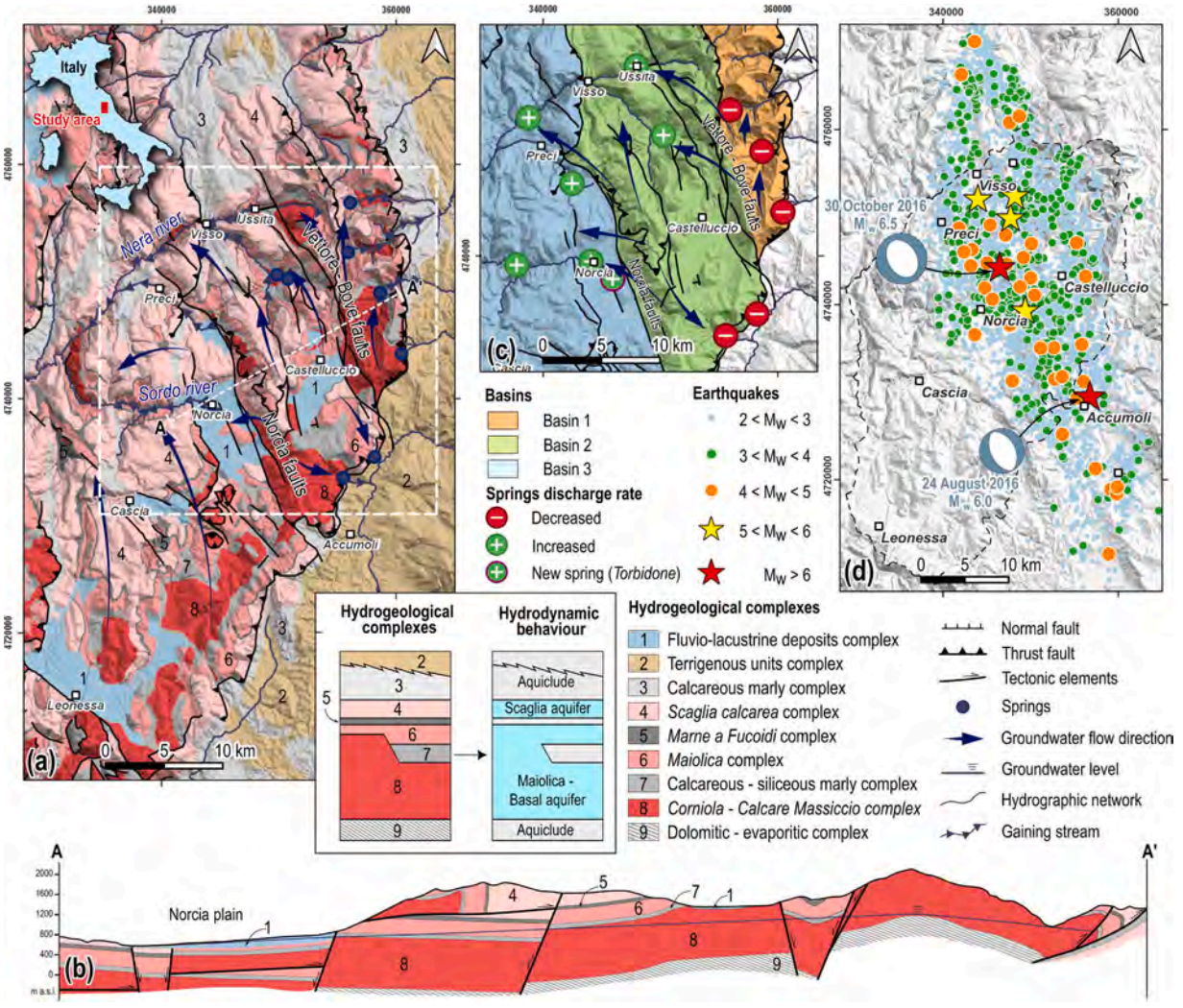

Fig. 1. Sketch of the study area. (a) hydrogeological and tectonic overview, together with the groundwater flow direction from tracer tests (Cambi et al., 2022) before the earthquake sequence (modified from Viaroli et al. (2021)). (b) Hydrogeological cross-section along the A-A' trace in panel a (modified from Viaroli et al. (2021)). (c) Detail of the area enclosed in the dashed grey rectangle in panel a, showing the increase and reduction of discharge rates measured at springs and spring groups after the 30th of October event (Valigi et al., 2020), together with the definition of the three basins constituting the regional hydrostructure and the groundwater flow direction after the earthquake sequence from tracer tests (Cambi et al., 2022). (d) The 2016 seismic sequence (data from Chiaraluce et al. (2017)). The dashed black line indicates the boundary of the *Sibillini* Mts hydrostructure.

from the Apennine foredeep (Pierantoni et al., 2013). Since the Early Pleistocene, SW-NE extensional tectonics have progressively dissected this compressive framework, creating intermontane Quaternary basins, such as *Norcia* and *Castelluccio*. The active extensional regime is evidenced by recent moderate seismicity and earthquake focal mechanisms (Pondrelli et al., 2006).

The hydrogeological framework of the *Sibillini* Mountains (Fig. 1a) is dominated by a multilayered carbonate aquifer system, characterised by a dual groundwater circulation: a deep, regional basal aquifer and a shallow aquifer system (Boni, 2010; Mastrorillo et al., 2009; Viaroli et al., 2021). The basal aquifer, the most productive and strategic, comprises fractured and karstified formations of the *Calcare Massiccio* and *Corniola* units (Lower Jurassic), as well as the *Maiolica* (Lower Cretaceous). Its flow is bounded below by the Triassic evaporitic sequence, which acts as a regional aquiclude (Fig. 1b). In this context, post-orogenic normal and transtensional faults, trending NW-SE and N-S, play a key role in modifying the regional hydrostructural framework, acting as either hydraulic barriers or conduits depending on the permeability of the fault zone. Indeed, groundwater flow in the basal aquifer primarily follows NNW–SSE to N–S structural trends and is compartmentalised by thrust faults that create hydrostructural barriers, and by extensional faults that can either impede or enhance flow (Cambi et al., 2022; Nanni et al., 2020; Nanni and Vivalda, 2005). The shallow aquifers develop within the *Scaglia Bianca* and *Scaglia Rossa* limestones (Upper Cretaceous–Paleogene) and are hydraulically separated from the basal system by the marly *Marne a Fucoidi* formation, which is spatially discontinuous and behaves as an aquiclude, where locally preserved. Porous aquifers hosted in Quaternary alluvial deposits fill tectono-karstic basins and are recharged by meteoric infiltration and lateral inflows from the carbonate massifs, favouring hydraulic connections with streams (Boni, 2010; Viaroli et al., 2021). Springs emerge naturally at structurally controlled locations, feeding both the Tyrrhenian and Adriatic catchments (Boni et al., 1991; Mastrorillo et al., 2009).

Groundwater circulation defines three main hydrostructural sectors (Fig. 1c), delimited by contractional and extensional structures and hydrostratigraphic contrasts (Mastrorillo et al., 2020; Nanni et al., 2020; Valigi et al., 2020). Although these sectors are physically distinct, hydraulic connectivity persists between them (Nanni et al., 2020; Valigi et al., 2020). The northward plunge of the *Vettore* Mt anticline, where the Triassic aquiclude crops out, serves as the principal piezometric divide between the Adriatic and Tyrrhenian groundwater flow domains.

2.2. The earthquake sequence

Such a hydrogeological context has been impacted by the 2016 earthquake sequence (Chiaraluce et al., 2017; Improta et al., 2019). The latter began on August 24th, with an M_w 6.0 earthquake located between *Accumoli* and *Amatrice* towns (Fig. 1d), followed two months later by an M_w 6.5 earthquake on October 30th, hitting *Norcia* town and causing further damage (Albano et al., 2019; Chiarabba et al., 2018; Tung and Masterlark, 2018). Thousands of aftershocks were registered during the seismic sequence, including four $M_w > 5$ events, spanning more than 850 km^2 (Fig. 1d).

The entire sequence developed along a normal fault system striking approximately NW-SE, dipping 40–55 ° SW-ward with a locally listric shape (Cheloni et al., 2019) and involving a crustal volume of roughly 6000 km^3 (Bignami et al., 2019). These faults crosscut the Earth's crust and outcrop along the *Vettore-Bove* fault system (Fig. 1a), which is characterised by extensional/transtensional kinematics and dissects the Meso-Cenozoic clayey/marly and carbonate sedimentary layers of the Central Apennines (Galadini and Galli, 2009).

3. Data analysis, conceptual modelling and numerical approach

The 2016 seismic sequence induced substantial hydrogeological changes in the carbonate aquifers of the *Sibillini* Mountains, particularly following the M_w 6.5 earthquake on October 30th, which affected the area northeast of *Norcia* (Boni et al., 1986; Mastrorillo et al., 2020; Petitta et al., 2022, 2021a, 2021b; Valigi et al., 2020, 2019; Viaroli et al., 2021). These changes included (Fig. 1c): i) a widespread increase in discharge from springs located on the western flank of the *Sibillini* Mountains and along the *Vettore-Bove* fault system, as well as in the main drainage network of the *Nera* River basin; ii) the reactivation of the *Torbidone* spring in the *Norcia* Plain, which had remained dry since 1979 (Petitta et al., 2018; Valigi et al., 2019); iii) a marked reduction in spring discharge on the eastern flank of the range, accompanied by a significant lowering of groundwater levels, which severely impacted the water supply infrastructures in the *Marche* region.

According to Mastrorillo et al. (2020), these hydrogeological anomalies, still observable today, can be attributed to a shift in the piezometric divide of *Vettore* Mt towards the east, because of the aquifer "rupture" caused by the fault dislocation. However, the underlying quantitative mechanisms responsible for this phenomenon have yet to be fully constrained. To address this gap, we developed a methodology to semi-quantitatively assess the impact of the seismic sequence on regional groundwater flow within the *Sibillini* hydrostructure.

We began by constructing a conceptual hydrogeological model of the study area. This model offered a first-order, qualitative framework for interpreting the aquifer's pre- and post-seismic behaviour. To inform this model, we integrated a comprehensive dataset from the literature, encompassing geological, tectonic, and hydrogeological maps; spring discharge time series; piezometric measurements from water wells and piezometers; hydrogeochemical analyses; and tracer test results acquired both before and after the seismic events.

Subsequently, we performed a numerical analysis to investigate the hydrodynamic response of the fractured carbonate aquifer system to the earthquake perturbations. The hydrogeological system was first simulated under steady-state conditions representative of the pre-seismic regime. This calibrated model was then employed to simulate steady-state groundwater flow immediately following the earthquake fault dislocation, enabling a semi-quantitative comparison of pre- and post-seismic hydrodynamic regimes.

3.1. Conceptual model and system behaviour

A conceptual model is a qualitative synthesis of current knowledge of the area, constructed from the available information. However, data limitations and knowledge gaps constitute the primary sources of (epistemic) uncertainty, which can influence the outcomes of the modelling process (Beven, 2016; Enemark, 2020). Despite these limitations, available literature data allowed the construction of the conceptual model in Fig. 2a.

The model is bounded by permeability limits that reflect tectonic and geometric boundaries. Tectonic boundaries include the *Sibillini* Mts thrust system, which provides hydraulic sealing due to its continuous and significant deformation zone along the NNE-SSW extent (Boni et al., 1986; Mastrorillo et al., 2012); and the *Coscerno* Mt thrust (CMt) to the southwest, serving as a local sealing feature according to Preziosi et al. (2022). Topographic and lithological limits mark the remaining boundaries. To the northwest, the upper-middle *Nera* River stands out as the lowest point in the area; it gathers groundwater from numerous springs primarily on its left bank, which leads to its classification as a hydraulic feature boundary. Finally, to the south, the hydrostructure is bounded by a groundwater divide close to the *Leonessa* municipality and the namesake normal fault system (Boni et al., 1986; Mastrorillo et al., 2009).

At depth, the basal limit of the hydrostructure is defined at the boundary between the *Calcare Massiccio* and the Triassic Evaporites formations (Fig. 1b), the latter being laterally continuous and acting as an effective seal unit when thrusted above Mesozoic carbonate/Tertiary units (Viaroli et al., 2021). This surface has been reconstructed by spatially interpolating the available hydrogeological cross-sections from Viaroli et al. (2021) and data from the 3D crustal model of Central Italy (Di Bucci et al., 2020; RETRACE-3D Working Group, 2021). Based on the above assumptions, the hydrogeological system covers approximately 1000 km^2. As shown in the cross-section in Fig. 2b, it exhibits variable thickness, generally decreasing from east to west with a mean value of around 1900 m.

Internally, groundwater flow direction is influenced by complex fault systems that disrupt both the vertical and lateral continuity of the aquifer layers, locally displacing the sequence and positioning at lateral contact horizons with different hydraulic properties.

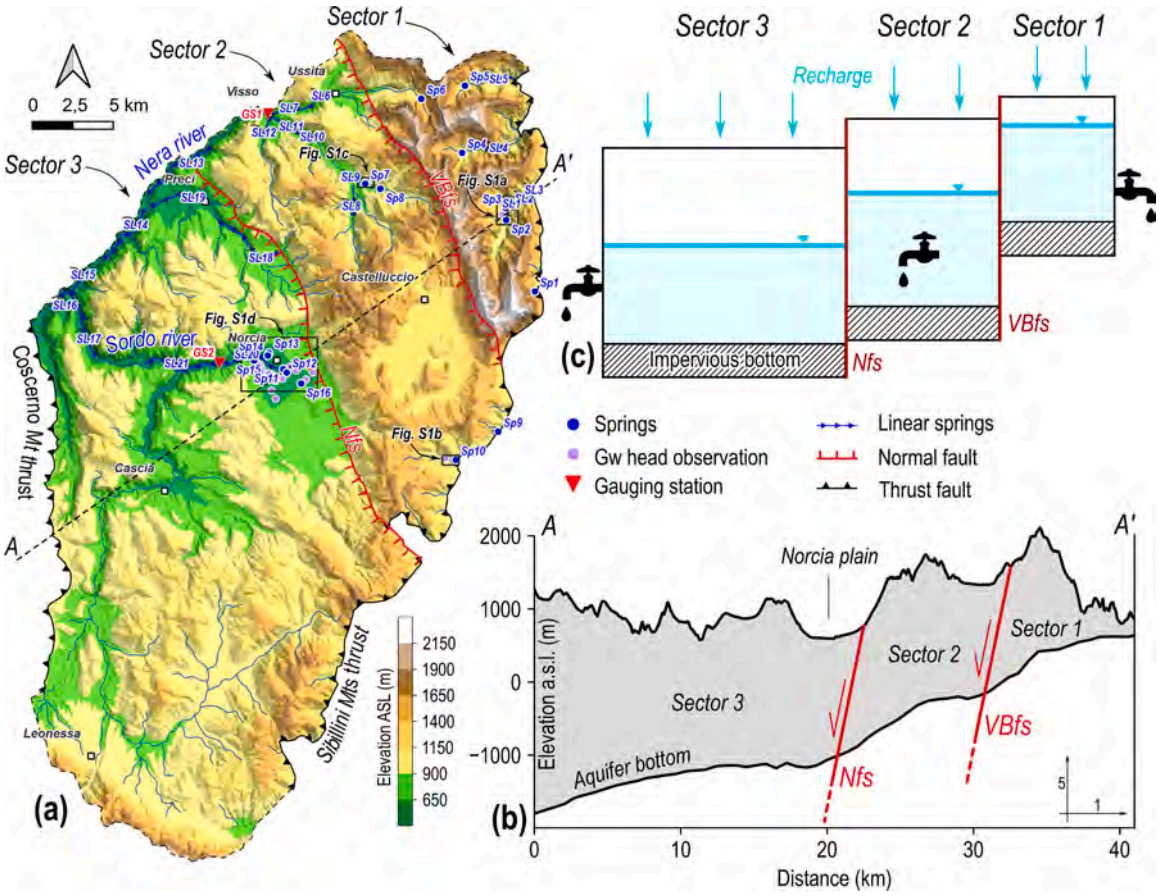

Fig. 2. (a) Regional hydrogeological conceptual model of the *Sibillini* Mts hydrostructure, with the location of punctual and linear springs, groundwater head observation points, and gauging station location along the main river courses. (b) Sketch of the cross-section of the hydrostructure along the A-A' trace in panel a, showing the top and bottom of the assumed homogeneous aquifer and the internal tectonic boundaries separating the three sectors. (c) The Idealised Box Model (IBM), representing the *Sibillini* hydrostructure in panel (a) as a basin-in-series scheme, where each sector is depicted as a reservoir, and a faucet symbolises linear and punctual springs.

Before the seismic sequence, tracer tests revealed that groundwater flow directions were nearly parallel to the *Vettore-Bove* (VBfs) and *Norcia* (Nfs) faults' strike (blue arrows in Fig. 1a) (Nanni et al., 2020), with only small amounts of cross-fault groundwater transfer. Hence, both fault systems acted primarily as barriers to groundwater flow directed orthogonally to their strike. We then incorporated VBfs and Nfs into the hydrogeological conceptual model as discrete features (Fig. 2b), which delineate a compartmentalised aquifer system divided into three main sectors, labelled Sector 1, 2 and 3 in Fig. 2a and b, approximately corresponding to the three basins defined in the literature (Valigi et al., 2020; Viaroli et al., 2021).

Such compartmentalization is further supported by the observation that, after the earthquake sequence, all the springs east of the VBfs exhibited a decrease in groundwater flow rate, while most of the springs west of the VBfs and Nfs experienced an increase in groundwater flow rate (Di Matteo et al., 2020; Fronzi et al., 2021; Petitta et al., 2018; Valigi et al., 2020, 2019), together with a change in groundwater flow directions, crossing both the VBfs and Nfs according to post-earthquake tracer tests (Cambi et al., 2022; Nanni et al., 2020), and then highlighting the active role of both fault systems in modulating groundwater flow rate and direction. The potential influence of other tectonic structures, such as secondary faults and thrusts within the *Sibillini* hydrostructure, has been disregarded because of their lesser relevance to the groundwater flow.

The largest amount of groundwater is stored in the *Corniola-Calcare Massiccio* hydrogeological formations (Fig. 1a), making the Basal Aquifer the most productive layer (Boni, 2010). Therefore, we considered the hydrogeological conceptual model consisting of a single aquifer layer.

Groundwater outflow occurs at several springs at different altitudes and along several river segments where the riverbed intersects the groundwater saturation level. In our conceptual model, we included the punctual and linear springs affected by the earthquake sequence, for which we have discharge data before and after the earthquake sequence (Fig. 2a and supplementary Table S1). Minor springs, representing less than 0.5 % of the total water budget, were neglected for modelling purposes. Additionally, data from wells and piezometers (Gw head observation points in Fig. 2a and supplementary Figure S1) have been incorporated to define the preseismic groundwater levels across the three basins (Mastrorillo et al., 2020; Petitta et al., 2022, 2021b; Valigi et al., 2020). The average piezometric values before the earthquake sequence are listed in Supplementary Table S2, while the available time series are shown in Figure S2.

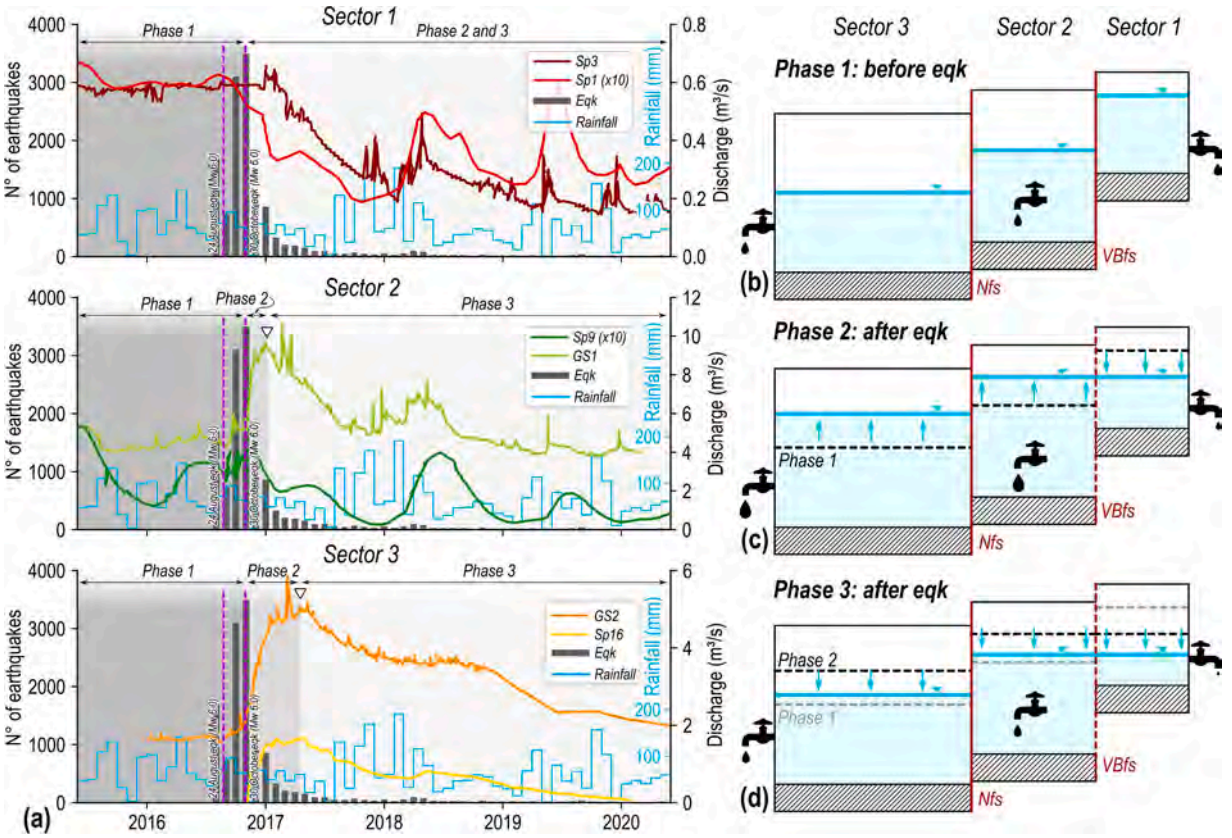

Fig. 3. (a) Discharge rate time series at monitored springs and gauging stations of the three sectors before and after the earthquake sequence, compared with the monthly seismicity rate and rainfall (seismicity from Chiaraluce et al. 2017, rainfall from the *Norcia* pluviometric station, available at https://annali.regione.umbria.it/). (b), (c) and (d) Schematic representation of the hydrodynamic behaviour of the *Sibillini* Mts hydrostructure employing the IBM in Fig. 2c, in three different phases before and after the 30 October 2016 earthquake, as highlighted in panel (a).

3.1.1. System behaviour before and after the earthquake sequence

Groundwater head and discharge variations are among the most direct manifestations of earthquake-induced perturbations. Therefore, to understand the hydrogeological system behaviour before and after the earthquake sequence, we examined the main springs, spring groups, and monitoring sites, which have nearly synchronous and homogeneous time series of recorded discharge and water-level fluctuations (Fig. 3a and Supplementary Figure S2).

The earthquake sequence began on August 24th, 2016, with an M_w 6.0 event located north of the *Accumoli* village (Fig. 1d). This event led to negligible changes in the discharge rate at the monitored springs and spring groups (Fig. 3a) and in piezometric levels (supplementary Figure S2). Otherwise, the M_w 6.5 earthquake on 30 October, located in the upper-central sector of the hydrostructure (Fig. 1d), caused widespread changes in discharge rates and groundwater head. Sector 1 experienced a rapid and substantial decrease in both spring discharge (Fig. 3a) and hydraulic head (supplementary Figure S2a). The Sp3 spring (*Foce di Montemonaco*, 910 m a.s.l.) showed a discharge reduction exceeding 55 %, dropping from 0.53 m^3 /s to below 0.24 m^3 /s. Simultaneously, piezometric monitoring within the *Aso* River catchment (panel a in Supplementary Figure S1) recorded a mean groundwater level decline of approximately 15 m (panel a in Supplementary Figure S2) (Petitta et al., 2022). A similar discharge decrease (~50 %) occurred at Sp1 spring (*Sassospaccato*, 1300 m a.s.l.), with flow rates falling from 0.06 m^3 /s to around 0.03 m^3 /s. Limited data from Sp4 spring (*Capotenna*, 1178 m a.s.l.) indicate a modest post-seismic reduction of about 8 %, from a pre-seismic average of 0.151 m^3 /s to approximately 0.139 m^3 /s.

In Sector 2, a moderate reduction in spring discharge was observed at high-elevation springs along the southeastern boundary of the hydrostructure (Sp9 and Sp10 in Fig. 2a). Because of their sensitivity to recharge and highly variable flow regimes, establishing reliable pre- and post-seismic discharge averages is challenging. Notably, Sp9 (Fig. 3a) (*Pescara spring*, ~ 891 m a.s.l.) showed an initial increase above the annual average discharge, followed by a progressive decline, with discharge decreasing from an estimated pre-seismic average of ~ 0.27 m^3 /s to ~ 0.14 m^3 /s by late 2020 (Valigi et al., 2020). Similarly, Sp10 (*Capodacqua* spring, ~ 850 m a.s.l., not shown) exhibited a brief post-seismic increase in discharge, resulting in an estimated surplus of ~ 4.1×10^6 m^3 (Cambi et al., 2022), relative to its pre-seismic average of ~ 0.38 m^3 /s (Petitta et al., 2021b). However, beginning in late 2017, a sustained reduction in discharge was observed, reaching an average of ~ 0.3 m^3 /s by the end of 2020 (Cambi et al., 2022; Petitta et al., 2021b). Piezometric data from monitoring wells and piezometers (panel b in Supplementary Figure S1) showed minimal changes in groundwater levels (panel b in Supplementary Figure S2), as the latter are also strongly influenced by seasonal oscillations (Petitta et al., 2021b).

In contrast, the low-elevation, northwestern part of Sector 2 exhibited marked increases in spring discharge. Discharge rate at the gauging station located along the *Nera* River, near the village of *Visso* (GS1, Fig. 3a) rose by ~82 % between 25 October and 12 November 2016, from ~ 5.1 m^3 /s to 9.3 m^3 /s (Valigi et al., 2020), the latter collecting the discharge contributions from all the upstream springs (Sp_6, Sp_7, Sp_8, Sl_6, Sl_7, Sl_8, Sl_9, Sl_{10}, Sl_{11}, and Sl_{12} in Fig. 2a and Table S1). Piezometric data from nearby monitoring wells (panel c in Supplementary Figure S1) indicated a significant rise in groundwater levels of ~ 2–7 m after the 30 October event (panel c in Supplementary Figure S2), peaking in December 2016, followed by a gradual decline that nonetheless remained above pre-seismic levels through 2017 (Mastrorillo et al., 2020). The subsequent recession phase (2017–2018) was characterised by a depletion rate nearly double that observed before the seismic sequence (Di Matteo et al., 2020).

In Sector 3, the October 30th, 2016, earthquake triggered a significant hydrological response in the *Norcia* basin. The resurgence of the *Torbidone* spring (Sp16 in Fig. 2a and Fig. 3a) was a clear indicator, reaching peak discharges of ~1.5 m^3 /s within three months post-event (Cambi et al., 2022; Checcucci et al., 2017; Petitta et al., 2018; Valigi et al., 2020, 2019). The total discharge measured at the gauging station along the *Sordo* River (GS2, Fig. 3a), which incorporates contributions from many springs (Sp11, Sp16, Sp12 and Sl20 in Fig. 2a and Table S1), peaked at ~5.8 m^3 /s, i.e., more than double the pre-seismic value of ~1.6 m^3 /s, before entering a gradual decline beginning around May 2018. In the *Norcia* plain, piezometric measurements based on pre- and post-seismic well surveys (panel d in Supplementary Figure S2) revealed almost stable groundwater levels in the preseismic phase (mean approximately 583 m a.s.l. during 2010–2011). After the seismic sequence, water table elevations increased by approximately 7 m, particularly in the eastern and southern sectors near the carbonate reliefs (panel d in Supplementary Figure S1), suggesting lateral groundwater transfer from Sector 2. Groundwater levels subsequently declined gradually until October 2019 (Valigi et al., 2020), although they remained above the pre-earthquake values.

3.1.2. Conceptual interpretation of observed data

To provide a simple yet effective interpretation of the observed variations in groundwater head and discharge rates, we developed an Idealised Box Model (IBM) as in Fig. 2c. In IBM, each box corresponds to one of the three sectors constituting the *Sibillini* Mts hydrogeological system, separated by the VBfs and Nfs faults, representing relative hydrogeological barriers. Rainfall infiltration serves as the recharge for each box, with its outflow represented by faucets, ideally symbolising the discharge of punctual and linear springs from each sector. We also assume a regional phreatic aquifer system (Nanni et al., 2020), in which changes in groundwater discharge correspond to changes in water levels within each box.

According to the available data, each sector shows a different hydraulic head level before the earthquake sequence (Phase 1 in Fig. 3b) (Nanni et al., 2020). The highest level is associated with the most topographically elevated Sector 1, while the lowest hydraulic head occurs in the most depressed Sector 3 (Supplementary Figure S2). Before the seismic sequence, groundwater mixing across the three Sectors is limited, as demonstrated by tracer tests (Cambi et al. 2022, and Fig. 1a), because the VBfs and Nfs act as relative hydrogeological barriers.

The 30 October event fault rupture extended through the entire hydrostructure to the surface (Cheloni et al., 2019; Villani et al., 2018), disrupting the seal between Sectors 1 and 2. This, in turn, triggered a transient diffusion process (Phase 2 in Fig. 3c and a), with the development of a groundwater wave travelling from Sector 1, first reaching Sector 2 and then Sector 3. This interpretation is

supported by the temporally delayed peak in discharge rates observed in these two sectors (the white triangles at the end of Phase 2 in Fig. 3a). Such a groundwater transfer explained the reduction in the groundwater head and discharge rate at Sector 1 (panel a in Supplementary Figure S2) and their initial, progressive increases at Sectors 2 and 3 (Fig. 3c and panels c and d in Supplementary Figure S2). The excess groundwater stored in Sector 1 was progressively discharged through existing punctual and linear springs located in Sectors 2 and 3, which consequently exhibited a temporary increase in discharge rates. Additionally, part of this surplus was released through the resurgence of previously inactive or newly formed discharge points, particularly along the gaining reaches of the Sordo and Nera rivers, as evidenced by the reactivation of the *Torbidone* spring in the *Norcia* Plain (Sp16 in Figs. 2a and 3a). This process persisted until the groundwater storage in Sector 1 was no longer sufficient to sustain the elevated discharge observed in Sectors 2 and 3. Indeed, rainfall infiltration alone was inadequate to maintain such enhanced post-seismic flow conditions in these sectors. Consequently, starting from approximately November 2017, both discharge rates and hydraulic heads in Sectors 2 and 3 began a gradual, long-term decline, similar to that observed in Sector 1 (Phase 3 in Fig. 3d; Supplementary Figure S2, panels a, c, and d). This decreasing trend persisted until 2020, eventually reaching magnitudes comparable to those before the earthquake. The attenuation of the decline in Sectors 2 and 3 can be attributed to their broader areal extent, which confers a higher hydraulic buffering (or lamination) capacity. In contrast, Sector 1 exhibits a persistent deficit in stored groundwater, reflecting a permanent transfer of groundwater toward Sectors 2 and 3.

From that point onward, discharge rates are mainly influenced by seasonal recharge dynamics, yet an overall downward trend persists throughout the whole hydrogeological system. This suggests that the available data do not identify a steady-state condition after the earthquake sequence.

3.2. Numerical modelling

We verified the proposed conceptual model and its behaviour before and after the seismic sequence through numerical simulations. We developed a steady-state model to simulate groundwater flow both before and immediately after the earthquake using the MODFLOW-OWHM (One-Water Hydrologic Flow Model) finite-difference code (Boyce, 2022; Boyce et al., 2020; Hanson et al., 2014). We adopted the Equivalent Porous Media (EPM) approach (Abusaada and Sauter, 2013; Lancia et al., 2020, 2018) to model a uniform, continuous aquifer layer.

We assigned a homogeneous initial hydraulic conductivity to the aquifer layer, assuming isotropy in the horizontal plane ($K_x = K_y$). We used the Newton Solver algorithm coupled with the Upstream Weighting package (UPW-NWT configuration) to solve the flow equation and ensure convergence, assuming unconfined conditions (Niswonger et al., 2011). Given this assumption, the base equation governing the two-dimensional, steady-state, groundwater flow simulation, accounting for the non-linearity introduced by the unconfined conditions (i.e. variable saturated thickness of cells), is expressed as:

$$\frac{\partial}{\partial x}\left(K_{aq}h\frac{\partial h}{\partial x}\right)+\frac{\partial}{\partial y}\left(K_{aq}h\frac{\partial h}{\partial y}\right)+W=0 \tag{1}$$

where K_{aq} is the aquifer's hydraulic conductivity (LT^{-1}), h is the hydraulic head (L), and W is the term related to inflow/outflow (LT^{-1}).

To simulate springs and riverbed springs that remove groundwater from the aquifer, we used the Drain (DRN) package (Harbaugh, 2005; McDonald and Harbaugh, 1984) (Eq. 2).

$$Q_{out} = C_d \bullet (h_d - h) \tag{2}$$

This head-dependent boundary enables the computation of the outflow leaving the cell Q_{out} (L^3T^{-1}), which depends on the drain conductance C_d (L^2T^{-1}) and the difference between the computed groundwater head h (L) and the drain's elevation h_d (L). Given that the drain conductance is a highly variable parameter influenced by the thickness and permeability of the riverbed material, it is typically estimated during calibration. Nevertheless, an initial uniform value was assumed for all drains.

The Recharge Package (RCH) allows water to enter the system (McDonald and Harbaugh, 1984). A uniformly distributed recharge equal to 1.62×10^{-8} m/s was estimated by dividing the total outflow from drains by the total area of the model A (L^2), maintaining the stationary water balance following the basic equation:

$$RCH = \frac{Q_{tot}}{A} \tag{3}$$

The Horizontal Flow Barrier (HFB) package (Hsieh and Freckleton, 1993) was used to model the VBfs and Nfs. This package simulates the presence of a hydraulic barrier by adding an additional conductance term to the flow computation between the two cells containing the barrier. This term depends on the barrier's hydraulic conductivity and thickness. Since this behaviour was assumed for both faults, a thickness of 1 m was assigned to each, based on the approximate mean range of fault cores from literature (Bense et al., 2013), and a hydraulic conductivity K_f (LT^{-1}) lower than that of the aquifer was assigned to both barriers.

Observation points were employed to compare model-generated values with experimental data. Specifically, the Drain Observation (DROB) and Head Observation (HOB) packages were implemented to record the simulated outflows from drain cells and track groundwater heads at designated locations within the model.

3.2.1. Numerical modelling rationale

Numerical analysis of post-earthquake hydrogeological changes requires defining the pre-earthquake hydrogeological conditions. For this reason, we started by modelling the steady-state groundwater flow of the *Sibillini* Mts hydrostructure before the earthquake sequence.

We began with a straightforward analysis of the system's operation and established an initial meaningful parametrisation. To achieve this, we first created a Semi-lumped Model (SM) by dividing the single aquifer layer into six rectangular cells, as shown in Fig. 4a.

SM dimensions were geometrically defined to preserve the actual size of the hydrostructure. The model top was set to the highest elevation relative to *Vettore* Mt (about 2476 m a.s.l.), while the bottom of the aquifer layer was set to −1000 m a.s.l., corresponding to the average depth inferred from the reconstructed bottom surface of the hydrostructure. Each domain sector is represented by a pair of adjacent cells aligned along the columns of the structured grid. We implemented both the VBfs and Nfs along the cells' boundaries, separating the three sectors of the model and functioning as hydraulic barriers (HFB1 and HFB2, respectively). Four drains were incorporated into the model cells to simulate the outflow points of the system. The drain lengths equal half the width of the cell in which they are placed, while their elevations were set to match the lowest representative spring level (meters a.s.l.) in each sector. The total outflow from each drain (q1, q21, q22 and q3) was determined by summing the discharge contributions from all the available springs and linear springs falling within each Sector (supplementary Table S1).

Additionally, head observations (h1, h21, h22, and h3) were assigned to the four model cells containing the head-dependent boundaries, represented by the DRN package. For each basin, a representative and feasible average hydraulic head observation value was selected from experimental data (supplementary Figure S2 and Table S2) to ensure that the head computed within the cell exceeds the drain elevation, thereby facilitating the proper functioning of the DRN package.

This Semi-lumped model served as an easy-to-use calibration tool to match both the experimental groundwater head and discharge rates before the earthquake sequence by adjusting the aquifer's hydraulic properties, the fault barriers, and the drains. To achieve this, we defined an initial hydraulic conductivity for both the aquifer (K_{aq}) and the fault barriers (K_f), along with an initial conductance value for the drains (C_d), as shown in Table 1, taking care that the fault permeability is not larger than the aquifer permeability ($K_f \leq K_{aq}$).

A first forward model was executed under steady-state conditions to simulate a preliminary pre-seismic groundwater flow and head. Then, initial values in Table 1 were refined through calibration using the PEST inversion algorithm (Doherty, 2015). The calibration was performed within the plausible parameter ranges (upper and lower values reported in Table 1) and using discharge rates from drains and groundwater head measurements as targets.

The best-fit parameter values obtained from the SM served as initial inputs for running a Distributed Model (DM) as in Fig. 4b, which accurately reproduces the conceptual model geometry presented in Fig. 2a. The DM has been discretised into square cells of

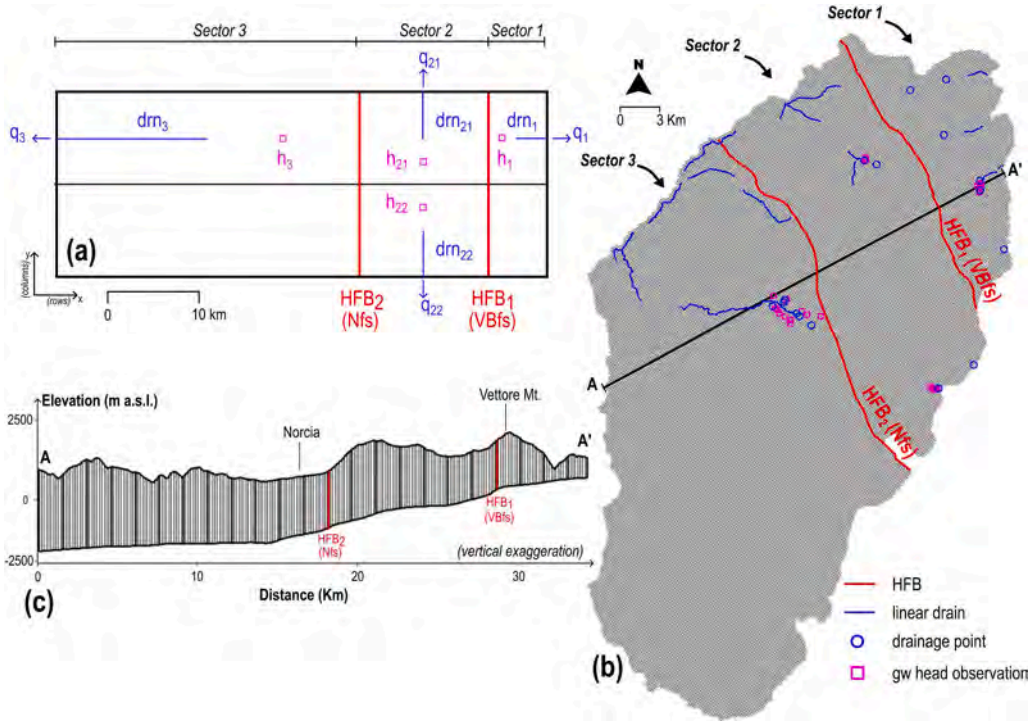

Fig. 4. Sketch of the developed numerical models of the *Sibillini* Mts hydrostructure: (a) Semi-lumped model (SM), (b) Plan view of the Distributed Model (DM) and (c) cross-section along the A-A' profile in panel (b).

Table 1
Initial, upper, and lower intervals of parameter values adopted for the SM and DM numerical models.

Feature	Package	Parameter	Initial value	Lower value	Upper value	unit
aquifer	-	K_{aq}	1×10^{-4}	1×10^{-9}	1×10^{-2}	m/s
fault barriers	HFB	K_f	1×10^{-12}	1×10^{-15}	K_{aq}	m/s
drains	DRN	C_d	1×10^{-2}	1×10^{-8}	1	m^2/s

150×150 m^2 resolution, oriented N28W to align with the average strike direction of normal fault systems. Both the VBfs and Nfs in Fig. 2a have been modelled with the HFB package (HFB1 and HFB2, respectively, in Fig. 4b) and the geometries and coordinates of all the springs and streambed springs in Fig. 2a have been imported and modelled as drains. The elevations assigned to the drains correspond to the elevations where they intersect the topography provided by the DEM. Drains in the same cell were combined into a single drain to avoid multiple identical boundary conditions. This is feasible because all those springs, very close to each other, drain water from the same Basal Aquifer.

Following the same approach as for the SM, we recalibrated the pre-earthquake DM parameters using the SM-calibrated values. We further inverted them using PEST, considering the ranges in Table 1 and using a larger number of discharge and head targets than in the previous SM calibration.

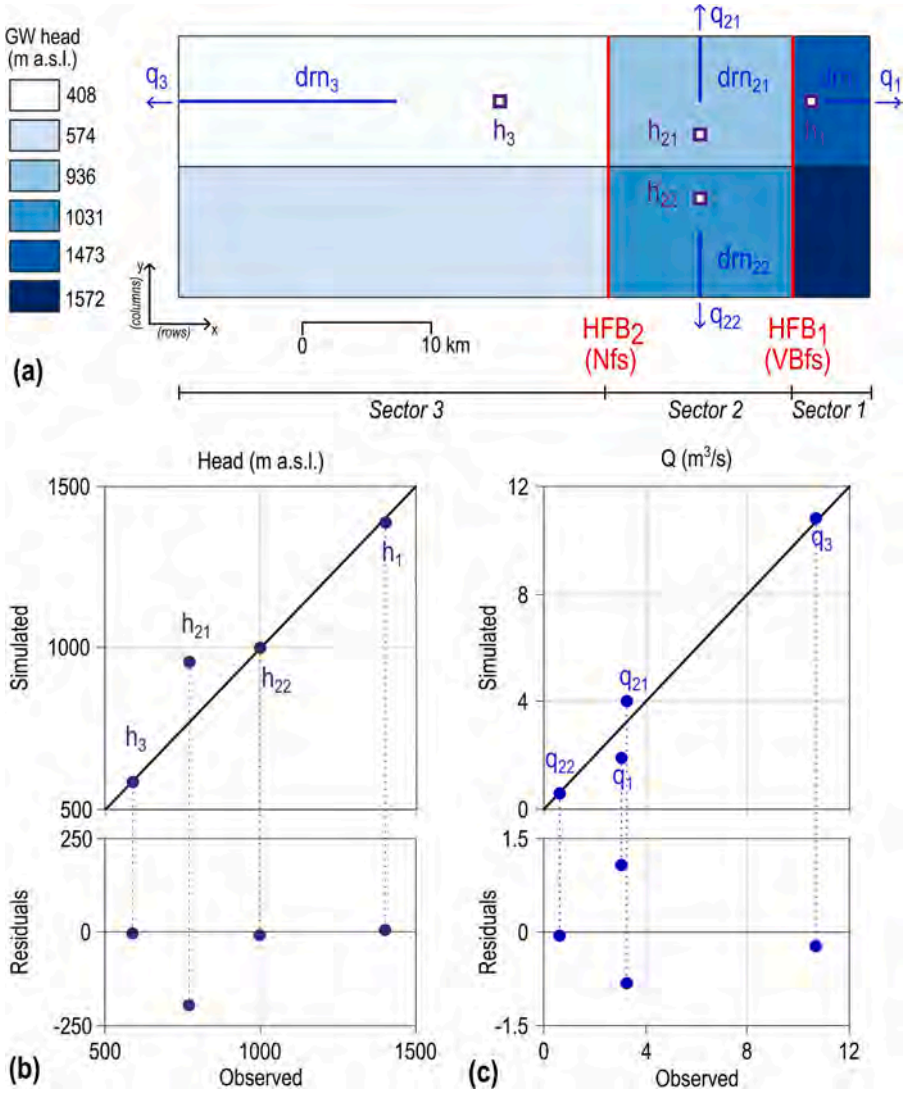

Fig. 5. Results of the steady-state groundwater flow model of the SM before the earthquake sequence. (a) distribution of the computed groundwater head. (b) and (c) Comparison between observed and simulated groundwater head (panel (b)) and discharge rates (panel (c)) at observation points, together with the residuals.

The optimised parameters obtained from the pre-earthquake DM were subsequently used to recompute groundwater flow in a steady-state forward simulation of the post-seismic scenario. In this case, we did not perform any inversion of the hydraulic parameters, as we cannot assume that current observations (Fig. 3a and Supplementary Figure S2) represent the steady-state conditions based on the available discharge rates and groundwater head data. No additional outflow boundaries were assumed beyond those explicitly defined within the DM domain for the pre-earthquake scenario. This modelling strategy is adopted to qualitatively investigate the short-term redistribution of groundwater flow and hydraulic head after the seismic event, rather than to reproduce the complete temporal evolution toward equilibrium.

We simulated only the fault rupture caused by the 30 October 2016 event, as this event resulted in the most widespread hydrogeological changes (Fig. 3a), by deactivating the HFB1 from the DM in Fig. 4a. With this approach, we remove the hydraulic barrier imposed by the VBfs prior to the earthquake, enabling a simplified simulation of the seismogenic fault rupture. Transient or permanent volumetric crustal changes due to seismic shaking and fault dislocation are not considered at this stage.

4. Numerical modelling results

The results of the numerical models are reported as hydraulic head maps and groundwater flow directions for both SM and DM, considering pre- and post-earthquake conditions.

4.1. Hydrogeological system before the earthquake sequence

4.1.1. SM results

The inversion results of the SM in Fig. 4a provided a schematic steady-state distribution of the hydraulic head across the different sectors of the idealised hydrostructure before the earthquake sequence, as in Fig. 5. The highest values occur in Sector 1, with an average maximum groundwater level of approximately 1572 m a.s.l. Sector 3 shows the lowest heads, around 408 m a.s.l., while Sector 2 exhibits intermediate levels, with a decreasing head gradient moving from south to north (h22 > h21). Such a result is consistent with observations. Indeed, simulated and experimental heads show an overall good fit, as in Fig. 5b, with larger residuals observed only for h21 in Sector 2 ($\Delta h > 100$ m), where simulated values are higher than observed values, which justifies a Mean Absolute Error (MAE) of 52.3 m. Regarding discharge rates (Fig. 5c), the fit between experimental and computed values is good, with an MAE of approximately 0.54 m^3/s. Larger residuals are still observed in Sector 2, where the q21 drain slightly overestimates the observed discharge rate, consistent with the overestimated groundwater head, and in Sector 1, where the simulated values are slightly lower than the observed ones. The best-fit hydraulic parameters of the SM, reported in

Table 2, fall inside the adopted ranges (i.e., lower and upper values in Table 1) and show permeabilities of the fault segments significantly lower than the aquifer, thus testifying to the role of a relative hydraulic barrier to the groundwater flow orthogonal to the fault strike. These values also agree with experimental ones from fault cores in Italy (Agosta et al., 2007; Ferraro et al., 2020).

4.1.2. DM results

Calibration of the DM prior to the earthquake sequence was conducted using a methodology analogous to that employed for the SM to determine optimal hydraulic parameter values. The initial parameterisation was based on the calibrated SM values (Table 2). Subsequently, inverse modelling was performed using PEST, incorporating observed groundwater heads and discharge rates (Supplementary Table S1) to refine the hydraulic parameters specific to the DM. The comparison between observed and simulated groundwater heads and discharge rates is presented in Supplementary Figure S3. Notably, the simulated groundwater heads are fairly consistent with those observed; however, the simulated discharge rates indicate the presence of inactive drains, which are situated at high elevations and exceed the modelled hydraulic head within the corresponding grid cells. The final set of best-fit parameters derived from the DM calibration is listed in Table 3. These parameters exhibit some deviations from those obtained for the SM but corroborate the influence of the Nfs and VBfs as relative hydraulic barriers.

The calibrated DM produced a more consistent and physically realistic simulation of pre-earthquake groundwater head distribution and flow patterns across the hydrostructure (Fig. 6a). Sector 1 is characterised by the highest computed hydraulic heads, ranging from approximately 1030 m a.s.l. beneath *Vettore* Mt to around 850 m a.s.l. in its northern extent. This spatial distribution of hydraulic head supports the conceptual hypothesis that the regional groundwater divide is situated within this sector, most likely associated with the structural high formed by the VBfs. The topographic and structural controls in this area result in a pronounced hydraulic gradient directing groundwater flow predominantly northeastward. This flow regime sustains the springs emerging along the northeastern

Table 2
Best-fit parameters estimated for the SM.

Object	Sector	Parameter	Best-fit value	Unit
aquifer	all	K_{aq}	6.32×10^{-6}	m/s
HFB1 (VBfs)	1–2	K_{f1}	1.00×10^{-12}	
HFB2 (Nfs)	2–3	K_{f2}	9.84×10^{-13}	
drn1	1	C_{d1}	2.93×10^{-3}	m^2/s
drn21	2 North	C_{d21}	1.22×10^{-2}	
drn22	2 South	C_{d22}	3.18×10^{-3}	
drn3	3	C_{d3}	1.73×10^{-1}	

Table 3
Best-fit parameters estimated for the DM. The "DRN" object defines the best-fit parameter for all drains falling into each Sector.

Object	Sector	Parameter	Best-fit value	Unit
aquifer	all	K_{aq}	1.69×10^{-5}	m/s
HFB1 (VBfs)	1–2	K_{f1}	8.91×10^{-13}	
HFB2 (Nfs)	2–3	K_{f2}	3.76×10^{-11}	
DRN	1	C_{d1}	4.97×10^{-1}	m^2/s
DRN	2 North	C_{d21}	1.70×10^{-4}	
DRN	2 South	C_{d22}	2.16×10^{-1}	
DRN	3	C_{d3}	3.11×10^{-3}	

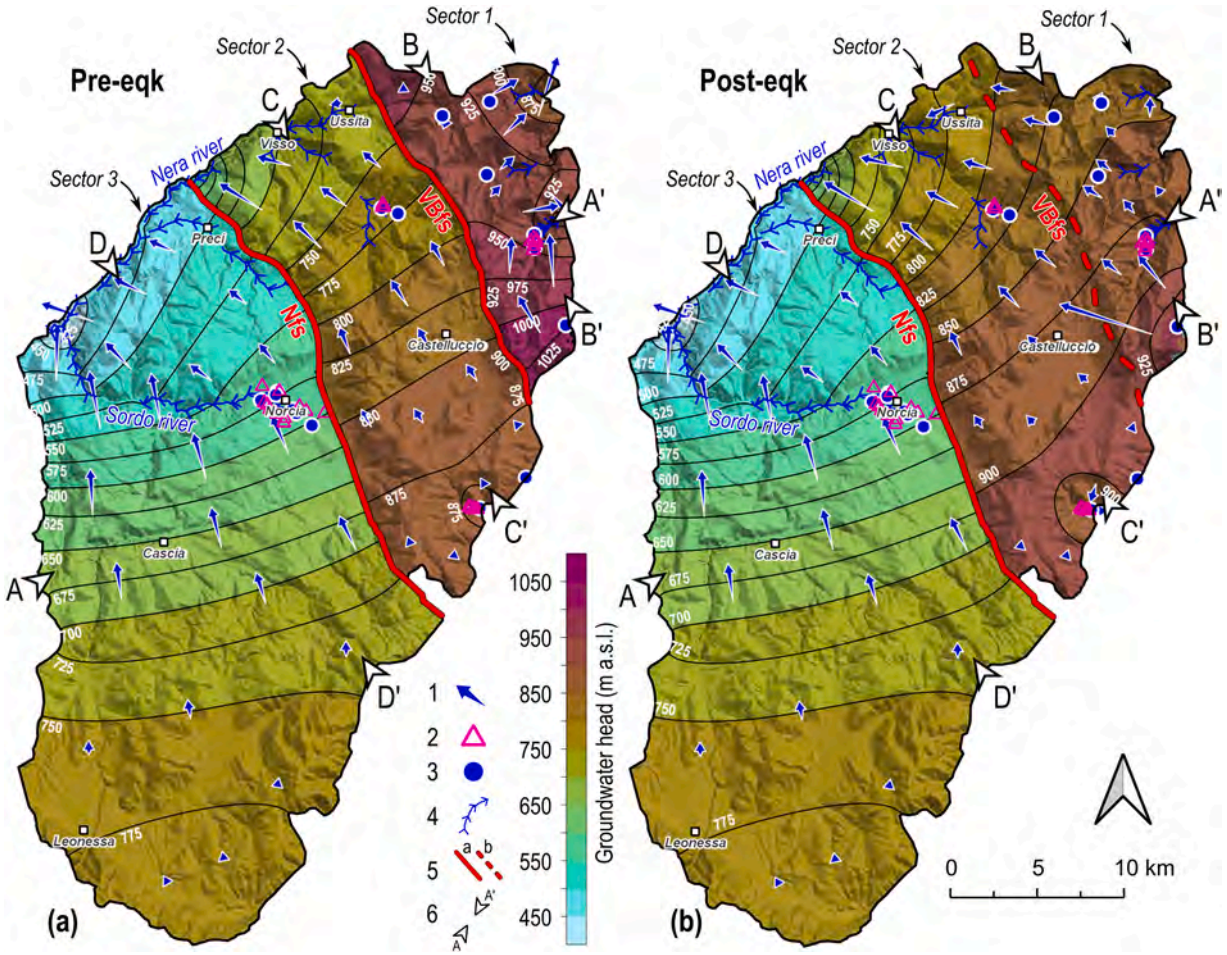

Fig. 6. Results of the steady-state DM of the *Sibillini* Mts hydrostructure, expressed in terms of groundwater head and flow directions, before (a) and after (b) the 30th of October 2016 earthquake. Key to the legend: 1) Modelled groundwater flow vectors; 2) Piezometric head observations; 3) Punctual spring discharge observations; 4) Linear springs discharge observations; 5) Internal boundary impervious relative to the surrounding rock (Nfs= *Norcia* Fault system; VBfs= *Vettore-Bove* fault system): (a) active, (b) inactive; 6) Trace of the cross-sections in Fig. 7a.

flanks of the hydrostructure.

The VBfs functions as a semi-permeable structural boundary, significantly influencing groundwater storage and flow dynamics. It promotes water accumulation in Sector 1, effectively creating a hydraulic contrast with the adjacent Sector 2. This contrast manifests as a marked head drop, evident in the cross-sectional view along transect A–A′ (Fig. 7a, dashed red line), and highlights the role of the VBfs as a relative hydraulic barrier.

In Sector 2, the simulated hydraulic heads reach approximately 875 m a.s.l., particularly in the *Castelluccio* Plain and *Capodacqua* (Sp10 in Fig. 2a) areas. These zones correspond to recharge and localised flow convergence areas, where the *Capodacqua* spring (Sp10) acts as a discharge point draining southward. The minimum head values in this sector, around 600 m a.s.l., occur near the *Visso* village, reflecting a significant downward gradient (Fig. 7a, Section C–C′, dashed red line). The dominant groundwater flow direction in this

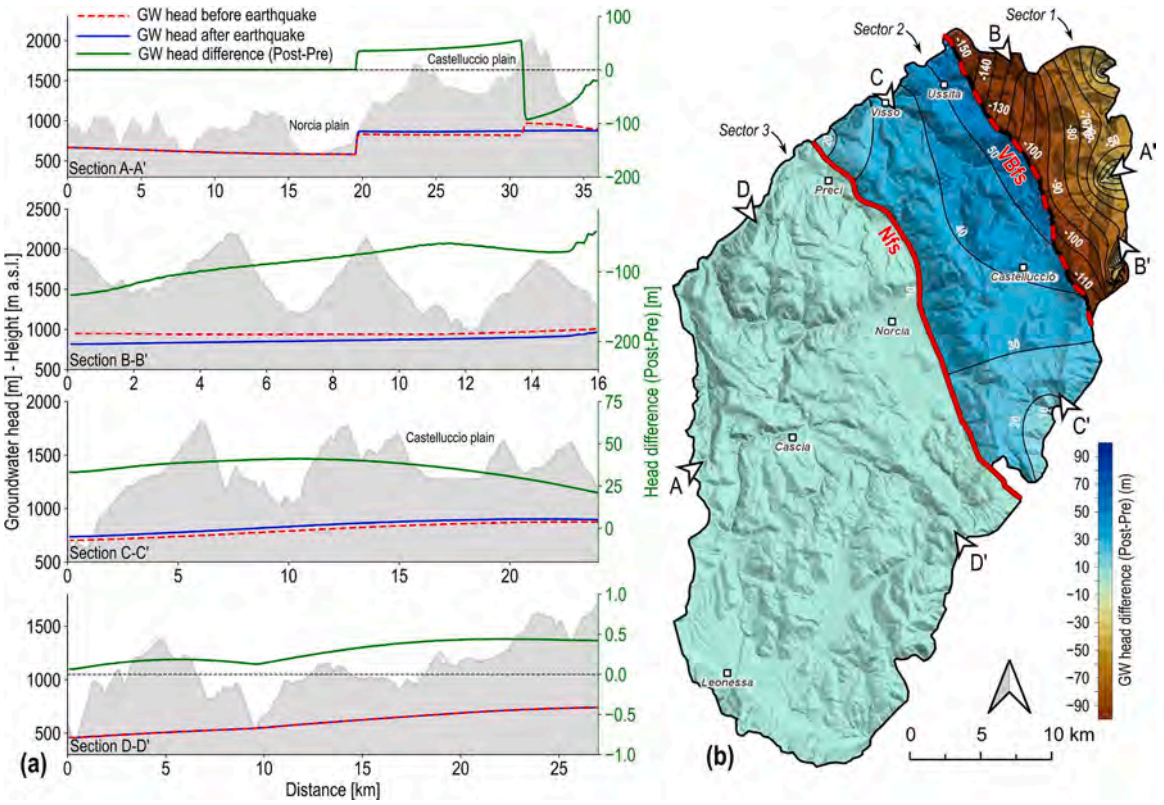

Fig. 7. Results of the DM before and after the earthquake. (a) Cross-sections reporting the groundwater table before and after the removal of the HFB1 corresponding to the VBfs, together with their difference (post−pre). The traces of the cross-sections are reported in Fig. 6a and b. (b) Plot of the difference between the groundwater head after (Fig. 6b) and before (Fig. 6a) the VBfs removal. For the legend of symbols in panel (b), please refer to Fig. 6.

central sector is toward the northwest, aligning closely with the Nfs and VBfs tectonic lineaments. These structural alignments guide the groundwater toward the northern portion of the *Nera* River catchment, reinforcing the concept of structural control on regional flow paths.

Sector 3 exhibits the lowest overall hydraulic heads, ranging from approximately 775–450 m a.s.l. (Fig. 7a, Section D–D′, dashed red line). Groundwater in this sector primarily discharges along the northwestern basin margin, contributing to the *Sordo* and *Nera* rivers, representing the main basal outflow systems of the hydrostructure. These rivers serve as key discharge zones for deep-seated, regionally integrated groundwater flow systems. The groundwater flow in this sector is also directed northwestward, consistent with the regional topographic gradient and structural framework.

The substantial differences in hydraulic head between Sectors 1, 2, and 3 indicate partial hydraulic compartmentalisation of the system, imposed by the barrier effect of VBfs and Nfs fault zones. This compartmentalisation leads to variations in storage, flow direction, and discharge behaviour across the three sectors. The orientation of groundwater flow pathways, which are generally aligned with the regional tectonic features, reinforces the influence of structural controls. These observations agree with hydrogeological models previously described in the literature (Cambi et al., 2022), emphasising the interplay between fault zone permeability and groundwater partitioning. Nevertheless, while the faults act as relatively low-permeability structures under pre-seismic conditions, they do not fully impede groundwater transfer. The presence of slightly curved equipotential lines near fault zones, orthogonal to the main fault traces, indicates that some degree of cross-boundary flow persists. This suggests that the VBfs and Nfs act as leaky barriers, allowing limited hydraulic connectivity between adjacent sectors. Such a configuration is characteristic of fault zones with internal heterogeneity, where fractured zones or fault gouge material may locally facilitate or impede flow. Therefore, while the sectors exhibit distinct hydraulic behaviours, they remain partially interconnected, forming a complex but integrated regional hydrogeological system.

4.2. *Hydrogeological system after the earthquake sequence*

The removal of the VBfs barrier (HFB1 in Fig. 4b) to simulate the coseismic fault dislocation associated with the October 30th seismic event led to substantial modifications in both groundwater head distribution and flow dynamics, particularly within Sectors 1 and 2 (Fig. 6b). The post-earthquake steady-state simulation reveals a significant hydraulic reconfiguration: the previously distinct

hydraulic heads in Sectors 1 and 2 have now become equilibrated, exhibiting a continuous gradient ranging from approximately 925 m a.s.l. in the southeastern portion to about 550 m a.s.l. in the northwestern portion. This homogenisation of the hydraulic gradient is most evident in the A-A' cross-section (Fig. 7a, blue curve), where the steep pre-seismic gradients, especially those adjacent to the VBfs, have flattened due to the removal of HFB1. In contrast, the barrier effect imposed by the Nfs remains intact between Sectors 2 and 3, as the current simulation does not incorporate any changes in permeability resulting from static or dynamic stress perturbations associated with the seismic sequence. Consequently, hydraulic compartmentalisation between these sectors is maintained in the post-seismic model.

In Sector 1, the groundwater flow direction, previously oriented toward the north-northeast and parallel to the VBfs, now shifts significantly toward the northwest (Fig. 6b), indicating cross-barrier flow through the area previously compartmentalised by the VBfs. This altered flow regime enhances discharge into the *Nera* River. The groundwater head differential between pre- and post-earthquake conditions, illustrated in Fig. 7b and in Section B–B' of Fig. 7a, reveals a substantial average head reduction in Sector 1 on the order of approximately −57 m. This decline in hydraulic head reduces discharge from high-altitude springs within the Sector. The total computed outflow from Sector 1 decreases by approximately −1.58 m^3/s in the post-earthquake scenario, with a reduction percentage of approximately 82 % respect to the pre-seismic state (Supplementary Table S3).

Sector 2 exhibits a marked increase in groundwater head following the removal of the VBfs. The C–C' cross-section in Fig. 7a and b indicate a post-seismic average head increase of approximately + 30 m relative to pre-earthquake conditions. This change in hydraulic head results in a substantial rise in discharge from the northwestern and southeastern drains within Sector 2, with an increase of approximately + 0.9 m^3/s, corresponding to a percentage increase of approximately 93 % with respect to pre-earthquake discharge rates (Supplementary Table S3). These changes indicate a redistribution of groundwater storage and flow pathways, driven by the hydrostructural modification imposed by fault dislocation.

Sector 3 appears less affected by the removal of the VBfs, with both the groundwater head and flow direction remaining directed toward the northwest. This is consistent with the model assumption of unchanged hydraulic properties along the Nfs and within the surrounding areas. However, since the Nfs is not completely impermeable, an increase in hydraulic head is still observed in Section D–D' (Fig. 7a), which can be attributed to the head rise in Sector 2 that propagates downstream into Sector 3. This intersectoral influence results in an average increase in hydraulic head of approximately + 0.06 m and in the computed discharge rates of about+ 0.6 m^3/s, corresponding to a percentage increase of 4.2 % relative to pre-seismic conditions (Supplementary Table S3).

Overall, these results highlight the critical role of fault zone permeability in governing groundwater flow and storage dynamics in fractured carbonate aquifers. The removal of the VBfs barrier illustrates how structural discontinuities, when altered by tectonic processes, can lead to large-scale reorganisation of regional groundwater systems, with significant implications for spring discharge rates, water resource availability, and hydrogeological hazard assessment.

5. Discussion

The modelling results provided a semi-quantitative interpretation of the observed behaviour of the *Sibillini* Mts hydrostructure before and after the earthquake sequence. The SM preseismic model results (Fig. 5) support the hydrogeological compartmentalisation proposed in the conceptual model (Fig. 2a), as the parameter inversion procedure yielded low relative permeabilities for the VBfs and Nfs features relative to the surrounding medium, thus computing distinct head gradients and limited connectivity between the three sectors of the hydrogeological system. In this model, faults are represented as homogenous, low-permeability linear features of fixed thickness and hydraulic conductivity, not accounting for variability typically encountered on fault zones in the field, which are anisotropic and heterogeneous and consist of a core and damage zone with complex hydraulic behaviour, alternating between acting as barriers or conduits depending on stress state, lithology, and rupture history (Bense et al., 2013).

Despite the adopted simplifications, the model reproduces the observed groundwater heads and spring discharge rates with good accuracy (Fig. 5b and c), though simulated heads are overestimated in Sector 2.1, and discharge rates are overestimated in Sector 2.1 and underestimated in Sector 1. These discrepancies likely arise from minor mismatches between the internal boundary separating Sectors 1 and 2 in the conceptual model and the structural configuration described by Valigi et al. (2020). According to this interpretation, the boundary in the northwestern portion of the aquifer is slightly shifted northeastward, following the *Vettore - Bove* Mt thrust rather than the *Vettore* Mt normal fault (Fig. 1c). This shift would assign the Sp6 spring to Sector 2 instead of Sector 1, decreasing the measured discharge in Sector 1 and increasing it in Sector 2.1. Such redistribution could explain the modelled underestimation of discharge in Sector 1 and the overestimation in Sector 2.1. However, given the limited discharge involved, this boundary adjustment is not expected to significantly affect the overall model performance.

The DM results provide a clearer picture of the functioning of the *Sibillini* Mts hydrostructure (Fig. 6a), confirming the internal compartmentalisation between the three Sectors, each characterised by distinct groundwater head values (Fig. 7a), with groundwater circulation directed north-northwestward and almost parallel to the VBfs and Nfs features, in agreement with the observation from tracer tests before the earthquake sequence (Cambi et al., 2022). The computed groundwater head values agree quite well with the observations (Supplementary Figure S3a), whereas the correlation for groundwater discharge remains poor across all three Sectors, especially for the discharge points located at high elevations, which mostly resulted in dry conditions (Supplementary Figure S3b and Table S3). This difference likely arises from limitations inherent in the modelling process, primarily related to the inability to discretise the hydrogeological system into multiple layers and to adequately represent high-altitude groundwater circulation confined within less permeable units. For example, Sector 1 is situated at the front of the *Sibillini* Mts thrust system, where local tectonic conditions are highly complex and likely result in the superposition of multiple hydrostratigraphic units with distinct hydraulic behaviours, as suggested by Mastrorillo et al. (2012) and Petitta et al. (2022). This configuration could explain the occurrence of high-elevation

springs. Given the limited knowledge of this complex structural setting and the impracticality of fully incorporating it into a regional-scale model such as the one developed here, the simulated groundwater head is consequently lower than the observed elevation of these high-altitude springs, depriving them of their drainage capacity. Nevertheless, the regional configuration and spatial distribution of the steady-state flow field are satisfactorily reproduced, effectively capturing the system's dominant hydrogeological patterns.

The earthquake sequence disrupted this equilibrium and altered groundwater circulation across the three sectors, as clearly evident from the groundwater discharge rates and head observations in Fig. 3a and Supplementary Figure S2. The most significant evidence of changes in aquifer dynamics is observed following the October 30th earthquake (M_w 6.5) (Fig. 3a and Supplementary Figure S2). In contrast, the second and third strongest events of the sequence, namely, the August 24th (*Amatrice*, M_w 6.0) and October 26th (*Visso* event, M_w 5.9), do not show clear signs of hydrological impact. Several factors contribute to this discrepancy. Firstly, the spatial locations of the earthquakes differ with respect to the October 30th event: the August 24th and October 26th events occurred at the eastern and western margins of the hydrogeological structure, respectively, whereas the October 30th event nucleated in the middle of the hydrostructure (Fig. 1d). Secondly, the August 24th and October 26th earthquakes released significantly less seismic energy than the October 30th event, and their associated fault ruptures likely did not propagate to the surface (Albano et al., 2016; Huang et al., 2017). As a result, the hydraulic integrity of the hydrogeological system remained largely unaffected.

In contrast, the October 30th earthquake caused well-documented surface ruptures, disrupting the aquifer system over at least 20 km, as evidenced by field surveys and remote sensing data (Bignami et al., 2019; Villani et al., 2018). This also suggests that transient shaking-induced hydrodynamic changes are minimal; if shaking alone was responsible for the observed hydrological changes, similar effects would be expected after the August 24th event. Therefore, we argue that the observed changes in aquifer behaviour primarily result from non-transient structural modifications. These include alterations in the aquifer's hydraulic properties due to fault rupture, breaching the hydraulic barrier between Sectors 1 and 2, and broader volumetric deformation of the crust.

Such a hypothesis is qualitatively confirmed by the post-earthquake numerical model shown in Fig. 6b, which simulated the earthquake rupture associated with the October 30th event by simply removing the VBfs as a hydraulic barrier in the distributed model, idealising the fault's mechanical failure and the resulting permeability enhancement. This approach treats post-seismic permeability enhancement as a binary change (i.e., barrier removal) rather than as a spatially distributed and stress-dependent adjustment. Despite such simplifications, the simulation produced a post-seismic redistribution of hydraulic heads and flow paths (Fig. 6b) that qualitatively matched observed changes, such as (i) the sudden decrease in groundwater head and discharge rates at eastern springs (Sector 1) and (ii) the rise in groundwater head and discharge in western and central areas (Sectors 2 and 3) (Fig. 7 and Supplementary Table S3). Such results are consistent with tracer test outcomes and field-measured trends in groundwater levels and flow rates (Mastrorillo et al., 2009; Nanni et al., 2020; Petitta et al., 2018; Valigi et al., 2019).

5.1. *Model limitations and potential solutions*

However, the amplitude of the computed discharge rates and groundwater head is quite different from those observed in the field, especially for Sectors 2 and 3. This is because the implemented steady-state model for post-seismic simulations simplifies the inherently dynamic, temporally variable hydrogeological rebalancing. Indeed, the model does not capture the transient propagation of pressure waves, delayed recharge-discharge cycles, the resurgence of new springs, or the evolving permeability due to time-dependent fracture opening, clogging, and modifications of karst networks. Consequently, while the model effectively reproduces an ideal steady-state scenario of discharge rates and hydraulic head, it currently cannot resolve short- to medium-term hydrodynamic adjustments, such as those observed in the weeks and months immediately following the earthquake (Fig. 3a). For this reason, the post-seismic scenario was simulated without recalibration, given the uncertainty regarding the achievement of a new hydrodynamic equilibrium in the field data (Fig. 3a). While this decision is methodologically sound, given the long, potentially incomplete transition to steady state, it limits the predictive power of the post-seismic simulations. The modelled changes should thus be interpreted as hypothetical end members of a dynamic evolution, rather than as precise forecasts of current conditions. To resolve such an issue, we can invoke the scalability of the proposed model approach by implementing a transient model based on the developed DM geometry. In this way, we can simulate the entire time series of discharge rates and hydraulic heads rather than defining an ideal steady-state condition based on the available data.

Finally, the absence of geomechanical coupling in the current model precludes the simulation of crustal volumetric strain and stress-induced variations in porosity and permeability along the fault plane and within the surrounding geological medium. This limitation is evident in the post-seismic model results presented in Fig. 6b and Fig. 7, where the predicted amplitudes of groundwater head and discharge rates differ significantly from those observed (Fig. 3a). This discrepancy can be attributed to two factors: (i) the modelled hydraulic fault behaviour, which is simply removed in the postseismic model rather than assuming a spatially distributed and stress-dependent permeability adjustment, and (iii) the absence of crustal volumetric deformation effects, which could modify aquifer properties beyond the fault zone. Several studies have demonstrated that seismic activity, through both dynamic (seismic wave propagation) and static (coseismic stress changes) mechanisms, can induce significant changes in aquifer hydraulic properties. These include variations in permeability, porosity, storage coefficients, and compaction (Albano et al., 2021b, 2021a, 2019, 2017; Nespoli et al., 2018; Tung and Masterlark, 2018). Such mechanical-hydrogeological interactions are particularly relevant in fractured and karst systems, such as the one analysed in this study. Specifically, the October 30th earthquake event induced measurable ground uplift and southwestward horizontal displacement across the Norcia Plain, resulting in dilatational crustal strains down to depths of approximately 1.5 km (Albano et al., 2021a). These volumetric strains likely enhanced permeability, facilitating the groundwater transfer from Sector 2 to Sector 3 across the *Norcia* fault.

To address this modelling shortcoming, a fully coupled hydro-mechanical model should be implemented. Such an approach would allow for the simulation of crustal stress redistribution, fracture dilation, and elastic deformation, thereby enabling a more comprehensive and physically realistic prediction of post-seismic volumetric changes both along the fault and in the surrounding rock, thus allowing for a more precise definition of fault and crustal permeability changes, for a better estimation of the hydrogeological response.

5.2. Possible long-term implications

Although the available data suggest that pre-earthquake conditions have been nearly re-established in Sectors 2 and 3, Sector 1 continues to exhibit a persistent decline in groundwater storage, with no evidence, at least so far, of trend reversal. This long-term depletion is attributed to the disruption of the hydraulic barrier previously exerted by the *Vettore* Fault, which caused a permanent modification in the inter-sectoral hydraulic connectivity and drainage configuration. Consequently, potential future hydrogeological scenarios largely depend on (i) the effective groundwater recharge that will occur over the coming years, which will determine the ability of the system to replenish the drained storage and (ii) the extent to which pre-seismic bulk permeability conditions can be restored within both the aquifer units and the fault zone (Cambi et al., 2022; Mammoliti et al., 2022; Mastrorillo et al., 2023; Petitta et al., 2021b; Valigi et al., 2020). The expected recharge rates are affected by considerable uncertainty under the current climate-change framework; however, no substantial deviation from the pre-seismic mean annual recharge is anticipated in the short term. The recovery of bulk permeability, on the other hand, is controlled by a complex interplay between damage and healing processes. Numerous studies have shown that coseismic fault slip and associated deformation typically induce a significant increase in permeability (Mitchell and Faulkner, 2008; Zhu and Wong, 1997; Zoback and Byerlee, 1975). Conversely, during the interseismic period, progressive fault healing mechanisms, such as gouge compaction, cementation, and pressure-solution transfer, tend to reduce permeability and re-strengthen the fault structure (Gratier et al., 2003; Im et al., 2019; Tenthorey et al., 2003). The rate of crack sealing and mineral reprecipitation is estimated to occur over timescales comparable to or longer than the recurrence interval of major earthquakes (Gratier et al., 2003), suggesting that recovering pre-seismic hydraulic conditions may require centuries to millennia.

Therefore, the persistent groundwater deficit observed in Sector 1 likely represents a long-lasting, if not irreversible, condition on human timescales, reflecting the combined effects of structural modification of the fault zone and limited short-term recharge capacity.

6. Conclusions

This study aimed to bridge the gap between qualitative hydrogeological observations and semi-quantitative, physically based simulations for evaluating the hydrodynamic effects of large seismic events on complex carbonate aquifer systems, specifically focusing on the ***Sibillini*** Mts hydrostructure affected by the 2016 earthquake sequence. The strength of the proposed approach lies in its combination of rigorous conceptual modelling and numerical parsimony. The latter comprises a modular approach, starting with the simplest model configuration (SM in Fig. 4a and Fig. 2c) to model the investigated hydrogeological system, which requires minimal parameters while preserving the hydrogeological information and the inferred system dynamics. This model has proven effective in providing a straightforward analysis of the system's functioning and in establishing meaningful parameterisation of the required parameters.

The complexity of the numerical model is increased through the SM by introducing further details, such as the full geometry of the hydrostructure, appropriately discretised to account for punctual and linear drains, and the full fault extent, resulting in the DM model as in Fig. 4b. In the DM, the adopted regional-scale analysis justifies homogenising the hydrostructure into a single continuous aquifer, enabling the application of the EPM approach and the simulation of a single groundwater flow, at the cost of lower precision in fitting observed head and discharge rates. Indeed, certain regions of the hydrostructure, particularly the deeper aquifer zones and fault cores, remain poorly characterised due to limited data availability and spatial distribution, which introduce uncertainties into parameterisation and, by extension, into model results.

Nonetheless, calibration of hydraulic parameters using inversion techniques (PEST) ensured that the results were not merely illustrative, within the limits of available and spatially distributed observational data.

Simulations showed that the earthquake-induced fault rupture enabled cross-fault groundwater transfer, resulting in ongoing depletion of the eastern aquifer sector (Sector 1) and increased discharge in the central and western sectors (Sectors 2 and 3). These findings demonstrate how seismic events can alter groundwater flow patterns in fractured carbonate systems, emphasising the vital role of tectonic structures in maintaining their hydrodynamic balance.

The model's scalability permits the integration of additional complexity, such as multi-stratigraphic aquifer configurations and hydraulically and geometrically heterogeneous fault zones, contingent on the availability of appropriate data. Moreover, this methodology presents a replicable framework for application in analogous seismotectonic environments worldwide. The approach is robust, grounded in empirical data, and yields results that align well with observed post-seismic hydrological changes.

Nonetheless, the study also highlights several limitations. Future developments should focus on incorporating transient flow dynamics and hydro-mechanical coupling to better capture the effects of seismic stress redistribution on aquifer properties. Improvements in fault zone characterisation, surface water-groundwater interaction modelling, and the resolution of data gaps would substantially enhance model fidelity and predictive capacity.

CRediT authorship contribution statement

Carlo Doglioni: Writing – review & editing, Validation. **Enrica Zullo:** Writing – original draft, Methodology, Formal analysis, Data curation, Conceptualization. **Michele Saroli:** Writing – review & editing, Supervision, Funding acquisition, Conceptualization. **Matteo Albano:** Writing – review & editing, Writing – original draft, Supervision, Methodology, Conceptualization. **Gabriel Testa:** Writing – review & editing, Validation, Supervision. **Marco Moro:** Writing – review & editing, Investigation, Funding acquisition. **Nicola Bonora:** Writing – review & editing, Supervision. **Marco Petitta:** Writing – review & editing, Investigation, Data curation, Conceptualization. **Thomas Reimann:** Writing – review & editing, Supervision, Methodology.

Declaration of Generative AI and AI-assisted technologies in the writing process

During the preparation of this work, the authors used ChatGPT in order to improve the readability and clarity of the manuscript. After using this tool, the authors reviewed and edited the content as needed and take full responsibility for the content of the published article.

Funding

This research did not receive any specific grant from funding agencies in the public, commercial, or not-for-profit sectors.

Declaration of Competing Interest

The authors declare that they have no known competing financial interests or personal relationships that could have appeared to influence the work reported in this paper.

Acknowledgments

The present work was carried out as part of XXXVII PhD cycle at the University of Cassino and Southern Lazio, funded by Istituto Nazionale di Geofisica e Vulcanologia.

Appendix A. Supporting information

Supplementary data associated with this article can be found in the online version at doi:10.1016/j.ejrh.2025.103063.

Data availability

Data will be made available on request.

References

Abusaada, M., Sauter, M., 2013. Studying the flow dynamics of a karst aquifer system with an equivalent porous medium model. Groundwater 51, 641–650. https://doi.org/10.1111/j.1745-6584.2012.01003.x.

Agosta, F., Prasad, M., Aydin, A., 2007. Physical properties of carbonate fault rocks, fucino basin (Central Italy): implications for fault seal in platform carbonates. Geofluids 7, 19–32. https://doi.org/10.1111/j.1468-8123.2006.00158.x.

Albano, M., Barba, S., Bignami, C., Carminati, E., Doglioni, C., Moro, M., Saroli, M., Samsonov, S., Stramondo, S., 2021a. Numerical analysis of interseismic, coseismic and post-seismic phases for normal and reverse faulting earthquakes in Italy. Geophys. J. Int. 225, 627–645. https://doi.org/10.1093/gji/ggaa608.

Albano, M., Barba, S., Bignami, C., Carminati, E., Doglioni, C., Moro, M., Stramondo, S., Saroli, M., 2021b. Three-dimensional numerical simulation of the interseismic and coseismic phases associated with the 6 April 2009, Mw 6.3 L'Aquila earthquake (Central Italy). Tectonophysics 798, 228685. https://doi.org/10.1016/j.tecto.2020.228685.

Albano, M., Barba, S., Saroli, M., Polcari, M., Bignami, C., Moro, M., Stramondo, S., Di Bucci, D., 2019. Aftershock rate and pore fluid diffusion: insights from the Amatrice-Visso-Norcia (Italy) 2016 seismic sequence. J. Geophys. Res. Solid Earth 124, 995–1015. https://doi.org/10.1029/2018JB015677.

Albano, M., Barba, S., Solaro, G., Pepe, A., Bignami, C., Moro, M., Saroli, M., Stramondo, S., 2017. Aftershocks, groundwater changes and postseismic ground displacements related to pore pressure gradients: insights from the 2012 Emilia-Romagna earthquake: the 2012 Emilia-Romagna Earthquake. J. Geophys. Res. Solid Earth 122, 5622–5638. https://doi.org/10.1002/2017JB014009.

Albano, M., Chiaradonna, A., Saroli, M., Moro, M., Pepe, A., Solaro, G., 2024. InSAR analysis of post-liquefaction consolidation subsidence after 2012 Emilia earthquake sequence (Italy). Remote Sens. 16, 2364. https://doi.org/10.3390/rs16132364.

Albano, M., Saroli, M., Moro, M., Falcucci, E., Gori, S., Stramondo, S., Galadini, F., Barba, S., 2016. Minor shallow gravitational component on the Mt. Vettore surface ruptures related to MW 6, 2016 Amatrice earthquake. Ann. Geophys. 59, 2. https://doi.org/10.4401/ag-7299.

Anderson, M.P., Woessner, W.W., Hunt, R.J., 2015. Applied Groundwater Modeling: Simulation of Flow and Advective Transport, second ed. Academic Press, London; San Diego, CA.

Bense, V.F., Gleeson, T., Loveless, S.E., Bour, O., Scibek, J., 2013. Fault zone hydrogeology. Earth Sci. Rev. 127, 171–192. https://doi.org/10.1016/j.earscirev.2013.09.008.

Beven, K., 2016. Facets of uncertainty: epistemic uncertainty, non-stationarity, likelihood, hypothesis testing, and communication. Hydrol. Sci. J. 61, 1652–1665. https://doi.org/10.1080/02626667.2015.1031761.

Bignami, C., Valerio, E., Carminati, E., Doglioni, C., Tizzani, P., Lanari, R., 2019. Volume unbalance on the 2016 Amatrice - Norcia (Central Italy) seismic sequence and insights on normal fault earthquake mechanism. Sci. Rep. 9, 4250. https://doi.org/10.1038/s41598-019-40958-z.
Boni, C., 2010. Hydrogeological study for identification, characterisation and management of groundwater resources in the Sibillini Mountains National Park (Central Italy). Ital. J. Eng. Geol. Environ. 21–39. https://doi.org/10.4408/IJEGE.2010-02.O-02.
Boni, C.F., Bono, P., Capelli, G., 1986. Schema Idrogeologico dell'Italia Centrale – A) Carta idrogeologica (scala 1:500.000); B) Carta idrologica (scala 1:500.000); C) Carta dei bilanci idrogeologici e delle risorse idriche sotterranee (scala 1:1.000.000). Mem. della Soc. à Geol. Ital. 35, 991–1012.
Boni, C., Falcone, M., Giaquinto, S., Martini, E., Zoppis, L., 1991. Risorse idriche sotterranee dei massicci carbonatici umbri. Le acque sotterranee in Umbria. Protagon Publ. GNDCICNR 413, 49–64.
Boyce, S.E., 2022. MODFLOW One-Water Hydrologic Flow Model (MF-OWHM) Conjunctive Use and Integrated Hydrologic Flow Modeling Software.
Boyce, S.E., Hanson, R.T., Ferguson, I., Schmid, W., Henson, W., Reimann, T., Mehl, S.M., Earll, M.M., 2020. One-water hydrologic flow model: A MODFLOW based conjunctive-use simulation software (U.S. Geological Survey Techniques and Methods). Tech. Methods.
Brodsky, E.E., Roeloffs, E., Woodcock, D., Gall, I., Manga, M., 2003. A mechanism for sustained groundwater pressure changes induced by distant earthquakes. J. Geophys. Res. 108, 2002JB002321. https://doi.org/10.1029/2002JB002321.
Cambi, C., Mirabella, F., Petitta, M., Banzato, F., Beddini, G., Cardellini, C., Fronzi, D., Mastrorillo, L., Tazioli, A., Valigi, D., 2022. Reaction of the carbonate Sibillini Mountains Basal aquifer (Central Italy) to the extensional 2016–2017 seismic sequence. Sci. Rep. 12, 22428. https://doi.org/10.1038/s41598-022-26681-2.
Checcucci, R., Mastrorillo, L., Valigi, D., 2017. Groundwater and earthquake: brief remarks about seismic effects on groundwater resources availability in Valnerina. ASITJGW 6. https://doi.org/10.7343/as-2017-259.
Cheloni, D., Falcucci, E., Gori, S., 2019. Half-graben rupture geometry of the 30 October 2016 M $_W$ 6.6 Mt. Vettore-Mt. Bove earthquake, Central Italy. JGR Solid Earth 124, 4091–4118. https://doi.org/10.1029/2018JB015851.
Chiarabba, C., De Gori, P., Cattaneo, M., Spallarossa, D., Segou, M., 2018. Faults Geometry and the Role of Fluids in the 2016–2017 Central Italy Seismic Sequence. Geophys. Res. Lett. 45, 6963–6971. https://doi.org/10.1029/2018GL077485.
Chiaraluce, L., Di Stefano, R., Tinti, E., Scognamiglio, L., Michele, M., Casarotti, E., Cattaneo, M., De Gori, P., Chiarabba, C., Monachesi, G., Lombardi, A., Valoroso, L., Latorre, D., Marzorati, S., 2017. The 2016 Central Italy seismic sequence: a first look at the mainshocks, aftershocks, and source models. Seismol. Res. Lett. 88, 757–771. https://doi.org/10.1785/0220160221.
De Luca, G., Di Carlo, G., Tallini, M., 2018. A record of changes in the Gran Sasso groundwater before, during and after the 2016 Amatrice earthquake, Central Italy. Sci. Rep. 8. https://doi.org/10.1038/s41598-018-34444-1.
Di Bucci, D., Buttinelli, M., D'Ambrogi, C., Scrocca, D., RETRACE-3D Working Group, 2020. RETRACE-3D project: a multidisciplinary collaboration to build a crustal model for the 2016-2018 Central Italy seismic sequence. BGTA. https://doi.org/10.4430/bgta0343.
Di Matteo, L., Dragoni, W., Azzaro, S., Pauselli, C., Porreca, M., Bellina, G., Cardaci, W., 2020. Effects of earthquakes on the discharge of groundwater systems: the case of the 2016 seismic sequence in the central Apennines, Italy. J. Hydrol. 583, 124509. https://doi.org/10.1016/j.jhydrol.2019.124509.
Doherty, J., 2015. Calibration and uncertainty analysis for complex environmental models. Water Numer. Comput. Brisb. Aust.
Emergeo Working Group, 2013. Liquefaction phenomena associated with the Emilia earthquake sequence of May–June 2012 (Northern Italy. Nat. Hazards Earth Syst. Sci. 13, 935–947. https://doi.org/10.5194/nhess-13-935-2013.
Enemark, T., 2020. Hydrogeological Conceptual Model Development and Testing. Flinders University, College of Science and Engineering.
Ferraro, F., Agosta, F., Prasad, M., Vinciguerra, S., Violay, M., Giorgioni, M., 2020. Pore space properties in carbonate fault rocks of peninsular Italy. J. Struct. Geol. 130, 103913. https://doi.org/10.1016/j.jsg.2019.103913.
Fronzi, D., Mirabella, F., Cardellini, C., Caliro, S., Palpacelli, S., Cambi, C., Valigi, D., Tazioli, A., 2021. The role of faults in groundwater circulation before and after seismic events: insights from tracers, water isotopes and geochemistry. Water 13, 1499. https://doi.org/10.3390/w13111499.
Fyfe, W.S., 1978. Fluids In The Earth's Crust: Their Significance In Metamorphic, Tectonic And Chemical Transport Process. Elsevier Science, Amsterdam.
Galadini, F., Galli, P., 2009. Paleoseismology of silent faults in the central Apennines (Italy): the Mt. Vettore and Laga Mts. Faults. Ann. Geophys. 46. https://doi.org/10.4401/ag-3457.
Gratier, J., Favreau, P., Renard, F., 2003. Modeling fluid transfer along California faults when integrating pressure solution crack sealing and compaction processes. J. Geophys. Res. 108, 2001JB000380. https://doi.org/10.1029/2001JB000380.
Hansen, W.R., Eckel, E., Schaem, W., Lyle, R.E., George, W., Chance, G., 1966. The Alaska earthquake, March 27, 1964. Field Investigations and Reconstruction Effort. (Professional Paper No. 541). The Alaska Earthquake. U.S. Geological Survey.
Hanson, R.T., Boyce, S.E., Schmid, W., Hughes, J.D., Mehl, S.M., Leake, S.A., Maddok, T.I., Niswonger, R.G., 2014. Geological Survey Techniques and Methods 6–A51 (Techniques and Methods). Techniques and Methods. One-Water Hydrologic Flow Model (MODFLOW-OWHM), U.S.
Harbaugh, A.W., 2005. MODFLOW-2005, The U.S. Geological Survey modular ground-water model—the Ground-Water Flow Process. U. S. Geol. Surv. Tech. Methods 6 A16 Tech. Methods.
Hsieh, P.A., Freckleton, J.R., 1993. Documentation of a computer program to simulate horizontal-flow barriers using the. U.S. Geological Survey's modular three-dimensional finite-difference ground-water flow model (USGS Numbered Series). Open-File Report.
Huang, M., Fielding, E.J., Liang, C., Milillo, P., Bekaert, D., Dreger, D., Salzer, J., 2017. Coseismic deformation and triggered landslides of the 2016 M_w 6.2 Amatrice earthquake in Italy. Geophys. Res. Lett. 44, 1266–1274. https://doi.org/10.1002/2016GL071687.
Im, K., Elsworth, D., Wang, C., 2019. Cyclic permeability evolution during repose then reactivation of fractures and faults. JGR Solid Earth 124, 4492–4506. https://doi.org/10.1029/2019JB017309.
Improta, L., Latorre, D., Margheriti, L., Nardi, A., Marchetti, A., Lombardi, A.M., Castello, B., Villani, F., Ciaccio, M.G., Mele, F.M., Moretti, M., The Bollettino Sismico Italiano Working Group, Battelli, P., Berardi, M., Castellano, C., Melorio, C., Modica, G., Pirro, M., Rossi, A., Thermes, C., Pagliuca, N., Spadoni, S., Arcoraci, L., Battelli, A., Lisi, A., Pizzino, L., Baccheschi, P., Cantucci, B., Sciarra, A., Bono, A., Marcocci, C., Lauciani, V., Mandiello, A., Pintore, S., Quintiliani, M., Frepoli, A., Colini, L., Pinzi, S., Scognamiglio, L., Basili, A., D'Addezio, G., Sgroi, T., Smedile, A., Montuori, C., Tardini, R., Tozzi, R., Monna, S., Miconi, L., Mariucci, M.T., Di Maro, R., 2019. Multi-segment rupture of the 2016 Amatrice-Visso-Norcia seismic sequence (central Italy) constrained by the first high-quality catalog of Early Aftershocks. Sci Rep 9, 6921. https://doi.org/10.1038/s41598-019-43393-2.
Ingebritsen, S.E., Manga, M., 2019. Earthquake Hydrogeology. Water Resour. Res. 55, 5212–5216. https://doi.org/10.1029/2019WR025341.
Isaya, D., De Luca, G., Di Carlo, G., Guerriero, V., Martorana, R., Tallini, M., 2025. Hydroseismograms at Gran Sasso aquifer, Central Italy, for earthquake hydrology studies. Sci. Rep. 15. https://doi.org/10.1038/s41598-025-96113-4.
Kresic, N., Mikszewski, A., 2012. Hydrogeological conceptual site models: data analysis and visualization. CRC Press.
Lancia, M., Petitta, M., Zheng, C., Saroli, M., 2020. Hydrogeological insights and modelling for sustainable use of a stressed carbonate aquifer in the Mediterranean area: From passive withdrawals to active management. J. Hydrol. Reg. Stud. 32, 100749. https://doi.org/10.1016/j.ejrh.2020.100749.
Lancia, M., Saroli, M., Petitta, M., 2018. A Double Scale Methodology to Investigate Flow in Karst Fractured Media via Numerical Analysis: The Cassino Plain Case Study (Central Apennine, Italy). Geofluids 2018, 1–12. https://doi.org/10.1155/2018/2937105.
Lavecchia, G., Minelli, G., Pialli, G., 1988. The Umbria-Marche arcuate fold belt (Italy). Tectonophysics 146, 125–137. https://doi.org/10.1016/0040-1951(88)90086-8.
Leone, G., Jourde, H., Esposito, L., Ginolfi, M., Ventafridda, G., Fiorillo, F., 2025. Daily spring discharge of a diffuse-flow karst system predicted by a lumped modeling approach. In: Fiorillo, F., Parise, M., Petitta, M., Leone, G., Liso, I.S., Lorenzi, V. (Eds.), Advances in Karst Science, Eurokarst 2024. Springer Nature Switzerland, Cham, pp. 41–47. https://doi.org/10.1007/978-3-031-84338-9_6.
Li, B., Shi, Z., Wang, G., Liu, C., 2019. Earthquake-related hydrochemical changes in thermal springs in the Xianshuihe Fault zone, Western China. J. Hydrol. 579, 124175. https://doi.org/10.1016/j.jhydrol.2019.124175.
Mammoliti, E., Fronzi, D., Cambi, C., Mirabella, F., Cardellini, C., Patacchiola, E., Tazioli, A., Caliro, S., Valigi, D., 2022. A holistic approach to study groundwater-surface water modifications induced by strong earthquakes: the case of Campiano catchment (Central Italy). Hydrology 9, 97. https://doi.org/10.3390/hydrology9060097.

Manga, M., 2001. Origin of postseismic streamflow changes inferred from baseflow recession and magnitude-distance relations. Geophys. Res. Lett. 28, 2133–2136. https://doi.org/10.1029/2000GL012481.
Manga, M., Beresnev, I., Brodsky, E.E., Elkhoury, J.E., Elsworth, D., Ingebritsen, S.E., Mays, D.C., Wang, C., 2012. Changes in permeability caused by transient stresses: Field observations, experiments, and mechanisms. Rev. Geophys. 50, 2011RG000382. https://doi.org/10.1029/2011RG000382.
Manga, M., Rowland, J.C., 2009. Response of Alum Rock springs to the October 30, 2007 Alum Rock earthquake and implications for the origin of increased discharge after earthquakes. Geofluids 9, 237–250. https://doi.org/10.1111/j.1468-8123.2009.00250.x.
Manga, M., Wang, C.-Y., 2015. Earthquake Hydrology. in: Treatise on Geophysics. Elsevier, pp. 305–328. https://doi.org/10.1016/B978-0-444-53802-4.00082-8.
Mastrorillo, L., Baldoni, T., Banzato, F., Boscherini, A., Cascone, D., Checcucci, R., Petitta, M., Boni, C., 2009. Quantitative hydrogeological analysis of the carbonate domain of the Umbria Region (Central Italy). Ital. J. Eng. Geol. Environ. 1, 137–155. https://doi.org/10.4408/IJEGE.2009-01.O-08.
Mastrorillo, L., Nanni, T., Petitta, M., Vivalda, P.M., Banzato, F., Palpacelli, S., 2012. Le risorse idriche sotterranee dell'alto bacino del fiume Aso (Parco Nazionale dei Monti Sibillini): studio idrogeologico e valutazione dello stato di utilizzazione. Eng. Hydro Environ. Geol. 195–206. https://doi.org/10.1474/EHEGeology.
Mastrorillo, L., Saroli, M., Viaroli, S., Banzato, F., Valigi, D., Petitta, M., 2020. Sustained post-seismic effects on groundwater flow in fractured carbonate aquifers in Central Italy. Hydrol. Process. 34, 1167–1181. https://doi.org/10.1002/hyp.13662.
Mastrorillo, L., Viaroli, S., Petitta, M., 2023. Co-Occurrence of Earthquake and Climatic Events on Groundwater Budget Alteration in a Fractured Carbonate Aquifer (Sibillini Mts.—Central Italy). Water 15, 2355. https://doi.org/10.3390/w15132355.
McDonald, M.G., Harbaugh, A.W., 1984. A modular three-dimensional finite-difference groundwater flow model, Open-File Report. U.S. Geological Survey.
Mitchell, T.M., Faulkner, D.R., 2008. Experimental measurements of permeability evolution during triaxial compression of initially intact crystalline rocks and implications for fluid flow in fault zones. J. Geophys. Res. 113, 2008JB005588. https://doi.org/10.1029/2008JB005588.
Montgomery, D.R., Manga, M., 2003. Streamflow and Water Well Responses to Earthquakes. Science 300, 2047–2049. https://doi.org/10.1126/science.1082980.
Moro, M., Saroli, M., Stramondo, S., Bignami, C., Albano, M., Falcucci, E., Gori, S., Doglioni, C., Polcari, M., Tallini, M., Macerola, L., Novali, F., Costantini, M., Malvarosa, F., Wegmüller, U., 2017. New insights into earthquake precursors from InSAR. Sci. Rep. 7, 12035. https://doi.org/10.1038/s41598-017-12058-3.
Muir-Wood, R., King, G.C.P., 1993. Hydrological signatures of earthquake strain. J. Geophys. Res. 98, 22035–22068.
Nanni, T., Vivalda, P.M., 2005. The aquifers of the Umbria-Marche adriatic region: Relationships between structural setting and groundwater chemistry. Boll. della Soc. à Geol. Ital. 124, 523–542.
Nanni, T., Vivalda, P.M., Palpacelli, S., Marcellini, M., Tazioli, A., 2020. Groundwater circulation and earthquake-related changes in hydrogeological karst environments: a case study of the Sibillini Mountains (Central Italy) involving artificial tracers. Hydrogeol. J. 28, 2409–2428. https://doi.org/10.1007/s10040-020-02207-w.
Nespoli, M., Belardinelli, M.E., Gualandi, A., Serpelloni, E., Bonafede, M., 2018. Poroelasticity and Fluid Flow Modeling for the 2012 Emilia-Romagna Earthquakes: Hints from GPS and InSAR Data. Geofluids 2018, 1–15. https://doi.org/10.1155/2018/4160570.
Niswonger, R.G., Sorab, P., Motomu, I., 2011. MODFLOW-NWT, a Newton formulation for MODFLOW-2005. U. S. Geol. Surv. Tech. Methods 6–A37.
Papathanassiou, G., Mantovani, A., Tarabusi, G., Rapti, D., Caputo, R., 2015. Assessment of liquefaction potential for two liquefaction prone areas considering the May 20, 2012 Emilia (Italy) earthquake. Eng. Geol. 189, 1–16. https://doi.org/10.1016/j.enggeo.2015.02.002.
Parsasadr, H., Mustafa, S., Golian, M., Bense, V., 2024. Development of a finite element groundwater flow model to test drainage management strategies for the expansion of the Dareh-Zar open pit mine, Iran. Hydrogeol. J. 32, 1145–1165. https://doi.org/10.1007/s10040-024-02792-0.
Petitta, M., Banzato, F., Barberio, M.D., 2021a. Sapienza" Università di Roma, Dipartimento di Scienze della Terra. Stud. Idrogeol. della captazione di Pescara Del. Tronto.
Petitta, M., Banzato, F., Barberio, M.D., 2021b. Studio idrogeologico della sorgente di Capodacqua del Tronto. Dipartimento di Sci. della Terra Lab. di Idrogeol. Quant. Sapienza Univ. à di Roma.
Petitta, M., Banzato, F., Barberio, M.D., 2022. Studio idrogeologico della captazione di Foce e del sistema sorgivo del fiume Aso. "Sapienza". Univ. à di Roma Dipartimento di Sci. della Terra Lab. di Idrogeol. Quant.
Petitta, M., Mastrorillo, L., Preziosi, E., Banzato, F., Barberio, M.D., Billi, A., Cambi, C., De Luca, G., Di Carlo, G., Di Curzio, D., Di Salvo, C., Nanni, T., Palpacelli, S., Rusi, S., Saroli, M., Tallini, M., Tazioli, A., Valigi, D., Vivalda, P., Doglioni, C., 2018. Water-table and discharge changes associated with the 2016–2017 seismic sequence in Central Italy: hydrogeological data and a conceptual model for fractured carbonate aquifers. Hydrogeol. J. 26, 1009–1026. https://doi.org/10.1007/s10040-017-1717-7.
Pierantoni, P., Deiana, G., Galdenzi, S., 2013. Stratigraphic and structural features of the Sibillini Mountains (Umbria-Marche Apennines, Italy). IJG 132, 497–520. https://doi.org/10.3301/IJG.2013.08.
Pondrelli, S., Salimbeni, S., Ekström, G., Morelli, A., Gasperini, P., Vannucci, G., 2006. The Italian CMT dataset from 1977 to the present. Phys. Earth Planet. Inter. 159, 286–303. https://doi.org/10.1016/j.pepi.2006.07.008.
Preziosi, E., Guyennon, N., Petrangeli, A.B., Romano, E., Di Salvo, C., 2022. A Stepwise Modelling Approach to Identifying Structural Features That Control Groundwater Flow in a Folded Carbonate Aquifer System. Water 14, 2475. https://doi.org/10.3390/w14162475.
Reilly, T.E., Harbaugh, A.W., 2004. Guidelines for Evaluating Ground-Water Flow Models (Scientific Investigations Report 2004-5038). Sci. Investig. Rep.
RETRACE-3D Working Group, 2021. Progetto RETRACE-3D - centRal italy EarThquakes integRAted Crustal modEl - Rapporto Finale. Zenodo. https://doi.org/10.5281/ZENODO.4604940.
Rojstaczer, S., Wolf, S., Michel, R., 1995. Permeability enhancement in the shallow crust as a cause of earthquake-induced hydrological changes. Nature 373, 237–239. https://doi.org/10.1038/373237a0.
Sato, T., Sakai, R., Furuya, K., Kodama, T., 2000. Coseismic spring flow changes associated with the 1995 Kobe Earthquake. Geophys. Res. Lett. 27, 1219–1222. https://doi.org/10.1029/1999GL011187.
Scharling, P.B., Rasmussen, E.S., Sonnenborg, T.O., Engesgaard, P., Hinsby, K., 2009. Three-dimensional regional-scale hydrostratigraphic modeling based on sequence stratigraphic methods: a case study of the Miocene succession in Denmark. Hydrogeol. J. 17, 1913–1933. https://doi.org/10.1007/s10040-009-0475-6.
Shi, Y., Liao, X., Zhang, D., Liu, C., 2019. Seismic Waves Could Decrease the Permeability of the Shallow Crust. Geophys. Res. Lett. 46, 6371–6377. https://doi.org/10.1029/2019GL081974.
ŞİMşek, C., Akinci, G., Fistikoğlu, O., Canli, K., SözbİLİR, H., Ayol, A., BİLgiÇ, E., 2024. Response of water resources to the Kahramanmaraş earthquakes (MW 7.7 and MW 7.6)that occurred on February 6, 2023, on the East Anatolian Fault Zone (Türkiye). Turk. J. Earth Sci. 33, 69–84. https://doi.org/10.55730/1300-0985.1899.
Tenthorey, E., Cox, S.F., Todd, H.F., 2003. Evolution of strength recovery and permeability during fluid–rock reaction in experimental fault zones. Earth Planet. Sci. Lett. 206, 161–172. https://doi.org/10.1016/S0012-821X(02)01082-8.
Tung, S., Masterlark, T., 2018. Delayed Poroelastic Triggering of the 2016 October Visso Earthquake by the August Amatrice Earthquake, Italy. Geophys. Res. Lett. 45, 2221–2229. https://doi.org/10.1002/2017GL076453.
Valigi, D., Cardellini, C, C., Mirabella, F., Tazioli, A., Petitta, M., Caliro, S., Cambi, C., Banzato, F., Beddini, G., Fronzi, D., Lacchini, A, A., Mastrorillo, L., Palpacelli, S., Sbarbati, C, C., Viaroli, S., 2020. Caratterizzazione dei sistemi idrogeologici del territorio umbro influenzato dagli eventi sismici del 26-30 ottobre 2016 e valutazione degli effetti del sisma sull'approvvigionamento idrico. Contrib. alla Ric.
Valigi, D., Mastrorillo, L., Cardellini, C., Checcucci, R., Di Matteo, L., Frondini, F., Mirabella, F., Viaroli, S., Vispi, I., 2019. Springs discharge variations induced by strong earthquakes: the Mw 6.5 Norcia event (Italy, October 30th 2016). ROL 47, 141–146. https://doi.org/10.3301/ROL.2019.25.
Viaroli, S., Mirabella, F., Mastrorillo, L., Angelini, S., Valigi, D., 2021. Fractured carbonate aquifers of Sibillini Mts. (Central Italy). J. Maps 17, 140–149. https://doi.org/10.1080/17445647.2021.1894252.
Villani, F., Civico, R., Pucci, S., Pizzimenti, L., Nappi, R., De Martini, P.M., the Open EMERGEO Working Group, 2018. A database of the coseismic effects following the 30 October 2016 Norcia earthquake in Central Italy. Sci. Data 5, 180049. https://doi.org/10.1038/sdata.2018.49.
Vorhis, R.C., Rexin, E.E., Coble, R.W., 1967. Hydrologic Effects of the Earthquake Of March 27,1964 Outside Alaska, The Alaska Earthquake Series. United States Government Printing Office, Washington.
Wakita, H., 1975. Water wells as possible indicators of tectonic strain. Science 189, 553–555. https://doi.org/10.1126/science.189.4202.553.

Wang, H., 2000. Theory of linear poroelasticity with applications to geomechanics and hydrogeology, Princeton series in geophysics. Princeton University Press, Princeton, N.J.

Wang, Chi-Yuen, Dreger, D.S., Wang, Chung-Ho, Mayeri, D., Berryman, J.G., 2003. Field relations among coseismic ground motion, water level change and liquefaction for the 1999 Chi-Chi ($M_w = 7.5$) earthquake, Taiwan. Geophys. Res. Lett. 30, 2003GL017601. https://doi.org/10.1029/2003GL017601.

Zhu, W., Wong, T., 1997. The transition from brittle faulting to cataclastic flow: permeability evolution. J. Geophys. Res. 102, 3027–3041. https://doi.org/10.1029/96JB03282.

Zoback, M.D., Byerlee, J.D., 1975. The effect of microcrack dilatancy on the permeability of westerly granite. J. Geophys. Res. 80, 752–755. https://doi.org/10.1029/JB080i005p00752.